5-2017

Developing Intuitive, Closed-Loop, Teleoperative Control of Continuum Robotic Systems

Chase Gilbert Frazelle
Clemson University, cfrazel@clemson.edu

Developing Intuitive, Closed-loop, Teleoperative Control of Continuum Robotic Systems

---

A Thesis
Presented to
the Graduate School of
Clemson University

In Partial Fulfillment
of the Requirements for the Degree
Master of Science
Electrical Engineering

---

by
Chase Gilbert Frazelle
May 2017

Accepted by:
Dr. Ian Walker, Committee Chair
Dr. Apoorva Kapadia
Dr. Richard Groff

Abstract

This thesis presents a series of related new results in the area of continuum robot teleoperation and control. A new nonlinear control strategy for the teleoperation of extensible continuum robots is described. Previous attempts at controlling continuum robots have proven difficult due to the complexity of their system dynamics. Taking advantage of a previously developed dynamic model for a three-section, planar, continuum manipulator, we present an adaptation control-inspired law. Simulation and experimental results of a teleoperation scheme between a master device and an extensible continuum slave manipulator using the new controller are presented. Two novel user interface approaches to the teleoperation of continuum robots are also presented. In the first, mappings from a six Degree-of-Freedom (DoF) rigid-link robotic arm to a nine degree-of-freedom continuum robot are synthesized, analyzed, and implemented, focusing on their potential for creating an intuitive operational interface. Tests were conducted across a range of planar and spatial tasks, using fifteen participant operators. The results demonstrate the feasibility of the approach, and suggest that it can be effective independent of the prior robotics, gaming, or teleoperative experience of the operator. In the second teleoperation approach, a novel nine degree-of-freedom input device for the teleoperation of extensible continuum robots is introduced. As opposed to previous works limited by kinematically dissimilar master devices or restricted degrees-of-freedom, the device is capable of achieving configurations identical to a three section continuum robot, and simplifying the control of such manipulators. The thesis discusses the design of the control device and its construction. The implementation of the new master device is discussed and the effectiveness of the system is reported.

Dedication

To my friends and family for supporting me as I continue my journey at Clemson University.

Acknowledgments

I would first like to thank Dr. Ian Walker and Dr. Apoorva Kapadia for giving me the initial opportunity to conduct research as an undergraduate student. I would not be where I am today without this opportunity, nor have the experiences I have gained thus far from the graduate program.

Special thanks go to Dr. Richard Groff for serving as the final member of my thesis committee.

I would also like to thank my peers for acting as a sounding board for ideas and for assisting in my research.

Finally, I would like to thank my family for supporting me as I pursue my goals.

Table of Contents

Title Page . . . . . **i**

Abstract . . . . . **ii**

Dedication . . . . . **iii**

Acknowledgments . . . . . **iv**

List of Tables . . . . . **vii**

List of Figures . . . . . **viii**

1 Introduction **1**
1.1 Teleoperation of Continuum Manipulators 2
1.2 Nonlinear Control of Continuum Manipulators 2
1.3 Thesis Overview 3

2 A Nonlinear Controller for Planar Continuum Robots **4**
2.1 Mathematical Model 4
2.2 Control Design 7
2.3 Controller Simulation 11
2.4 Experimental Implementation 15
2.5 Discussion 16

3 New Results in Teleoperation of Continuum Robots **24**
3.1 The System 24
3.2 Input Mappings 27
3.3 Study Design 31
3.4 Experimental Results 36
3.5 Discussion 38

4 A Kinematically-Similar Master Device for Extensible Continuum Manipulators 41
4.1 Design and Construction 41
4.2 System Implementation 45
4.3 Discussion 46

5 Conclusion **51**
5.1 Summary of Contributions 51
5.2 Future Research 52

Appendices **54**

A Teleoperation Trial Documents 55

Bibliography 58

List of Tables

2.1 Kinematic Values for Experimental OctArm Configurations 15
2.2 λ Values Corresponding to Experimental Configurations 22
2.3 State Estimation Error [m] 22

3.1 Variable Mappings For Planar Motion 27
3.2 Variable Mappings For Spatial Motion 29
3.3 Completion Percentage for Each Spatial Mapping 38

List of Figures

2.1 The 9 Degree-of-Freedom OctArm Manipulator 5
2.2 Geometric Representation of s and κ for Continuum Section 5
2.3 OctArm Coordinate System 12
2.4 Master System Tracking Error 12
2.5 Jacobian Controlled Slave System Tracking Error 12
2.6 Slave System Tracking Error, λ=1 13
2.7 Slave System Tracking Error, $\lambda = 5$ 13
2.8 Slave System Tracking Error, $\lambda = 15$ 14
2.9 Slave System Tracking Error, $\lambda = 25$ 14
2.10 System Response with added White Gaussian Noise, SNR = 30 dB 14
2.11 Straight Configuration Tracking and Error Data 16
2.12 Curving Base Section Configuration Tracking and Error Data 17
2.13 Curving Middle Section Configuration Tracking and Error Data 18
2.14 Curving Tip Section Configuration Tracking and Error Data 19
2.15 All Sections Curving Configuration Tracking and Error Data 20

3.1 The 6 Degree-of-Freedom Kinova Mico Research Arm 25
3.2 Teleoperative Control Block Diagram 26
3.3 Orientation Based Tasks for Planar Motion Study 34
3.4 Task Phase of Spatial Motion Study 35
3.5 Average and Standard Deviation of Planar Mapping Evaluations 37
3.6 Average and Standard Deviation of Spatial Mapping Evaluations 37

4.1 MiniOct Continuum Controller 42
4.2 Cross Section of Push Tab System 43
4.3 Acrylic Spacer for Base Section of MiniOct 44
4.4 Ring of String Pots for Determining Configuration 44
4.5 Color Coordination of Base, Middle, and Tip Sections 46
4.6 Configurations between Master and Slave Device 47
4.7 Three Section Control of Slave Device 48

Chapter 1

Introduction

Teleoperation has traditionally been, and remains, a key enabling element in implementation of many robotic systems, and is particularly important in many safety-critical operations and unstructured environments [1]. Teleoperation of robot manipulators has been the subject of extensive research through the years [1]. However, almost all the related literature on teleoperation of manipulators applies to conventional rigid-link robot structures. In this thesis, we consider the teleoperation of continuum robots.

Continuous backbone, or continuum robots [2], differ fundamentally from traditional rigid-link robot structures, due to their ability to change shape (bend) at any point along their structure. Inspired by invertebrate morphologies in nature (tongues, trunks, and tentacles), their structures give them the ability to penetrate environments and perform tasks convention robots cannot [3], [4]. Over the past twenty years or so, an ever-increasing number and variety of continuum robots have been designed and implemented [5]. They have found applications in numerous medical procedures [6], [7], [8], inspection operations [9], space [10], [11], and underwater environments [12], [13].

The state-of-the-art in the modeling and operation of continuum robots has advanced rapidly in the past few years. The kinematics of continuum robots has been extensively studied [14], [15]. Research specific to continuum robots in areas traditional to robotics such as dynamics [16], [17], [18], [19], [20], [21], contact modeling [22], [23], motion planning [24], [25], [26], [27], and control [28], [29], [30], [31], [32], [33] is currently very active. However, little attention has been paid to the issue of user interfaces for, and in particular teleoperation of, continuum robots [5]. Human operation of continuum robots is hampered by the fact that their movements are typically significantly less intu-

itive to operators than those of their rigid-link counterparts. A limiting factor on the teleoperation of continuum robots has been the lack of intuitive relationship between a human interface and the continuum system.

1.1 Teleoperation of Continuum Manipulators

In the literature, there are three examples of teleoperation schemes concerning continuum manipulators. In [34], a traditional gaming joystick was mapped to the motions of a nine degree of freedom (DoF) continuum robot. A series of mappings were created and tested. Though the system was functional, the limited degrees of freedom of gaming joysticks (two or three degrees-of-freedom) created difficulties in translating the movements of the joystick to the movements of the continuum manipulator. In [35], a non-redundant rigid-link master was used to control the end effector of a planar continuum robot. This system did not directly control the 6 DoF available to the planar continuum manipulator, using instead the inverse Jacobian to determine the necessary control values to reach a desired point. Though this approach is useful, it does not take into account the environment of the manipulator and cannot be used in applications such as whole arm manipulation [36]. The final related piece of literature was a recent work detailing a software interface that allowed for the teleoperation of continuum manipulators through a graphical representation of the physical manipulator [37]. All of these investigations demonstrated useful capabilities in the teleoperation of continuum robots but each had numerous shortcomings, especially concerning intuitive control.

1.2 Nonlinear Control of Continuum Manipulators

Nonlinear control techniques are well established for robotic systems [38], [39], [40]. However, research into the nonlinear control of continuum systems is very limited in the literature. To the authors' knowledge, only one work [41] describes the investigation of model-based nonlinear control methods applied to continuum manipulators. In [41], a sliding-mode controller is developed. The results of the reported simulations show successful control of the continuum model and trajectories reaching the desired switching surface. Experiments in [31] further tested the performance of the previous sliding mode controller by comparing the results to that of a proportional-derivative (PD) controller. However, there are still numerous aspects of nonlinear control theory that have yet to be

investigated with regard to continuum robotic systems.

1.3 Thesis Overview

This thesis presents a series of efforts centered around enabling effective and intuitive teleoperation of continuum manipulators. The thesis is organized as follows. Chapter 2 introduces a nonlinear control law developed to create exponential tracking error convergence between the end-effector of a master device and a continuum slave manipulator in their respective environments. Chapter 3 considers and demonstrates the teleoperation of continuum robots using rigid-link manipulators as input devices. Chapter 4 describes the design, inspiration, and contruction of the MiniOct, a new and novel teleoperation input device designed for the purpose of intuitive continuum manipulator control. Chapter 5 presents conclusions drawn from the presented work and opportunities for future research.

Chapter 2

A Nonlinear Controller for Planar Continuum Robots

The inherently nonlinear nature of continuum robotic systems creates a unique problem when applying traditional control techniques. Nonlinear control techniques offer potential solutions to the control of continuum robots, including teleoperation. In [41], the authors demonstrate the effectiveness of sliding mode control in manipulating the end-effector position of the three-section continuum robot. This work exemplifies the usefulness of nonlinear controllers, but does not account for the numerous other control techniques that could be used for such systems.

In this chapter, we introduce a nonlinear control law developed to create asypmtotic tracking-error convergence between the end-effector of a rigid-link master system and a continuum slave system in their respective environments. The approach is inspired by traditional adaptive control techniques, but without the need to approximate unmodeled parameters.

2.1 Mathematical Model

In order to develop the nonlinear control law, we make use of both kinematic and dynamic models of an extensible continuum manipulator limited to a single plane of motion. Specifically, we use the model of a three section, 9 Degree-of-Freedom (DoF) extensible continuum manipulator referred to as the OctArm [42], seen in Figure 2.1. The OctArm is a kinematically redundant exten-

sible continuum robot comprised of three serially connected sections. The sections are designated as the base, middle, and tip, pictured from right to left, respectively, in Figure 2.1. Each section is capable of three independent motions: change in section length, change in section curvature, and change in orientation in three-dimensional (3D) space.

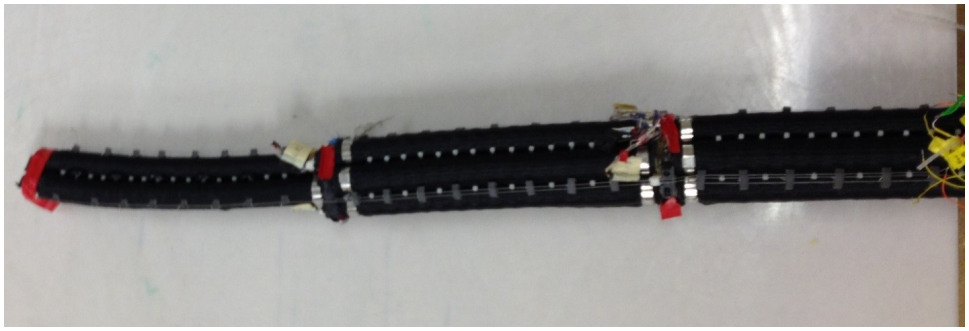

Figure 2.1: The 9 Degree-of-Freedom OctArm Manipulator

The 9 DoF available are $q = [s_1\ s_2\ s_3\ \kappa_1\ \kappa_2\ \kappa_3\ \phi_1\ \phi_2\ \phi_3]^{\mathrm{T}}$. As discussed in [14], $s_i(t)$ represents the section length, $\kappa_i(t)$ the section curvature, and $\phi_i(t)$ is the section orientation of the ith section, where i=1, 2, 3. When limited to a single plane, the number of DoF reduces from nine to six, resulting in $q(t) = [s_1\ s_2\ s_3\ \kappa_1\ \kappa_2\ \kappa_3]^{\mathrm{T}}$. Figure 2.2, from [14], depicts the geometric representation of s and κ for a single continuum section.

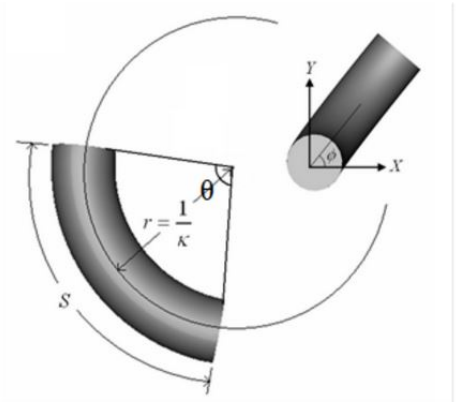

Figure 2.2: Geometric Representation of s and κ for Continuum Section

There were two master devices used in this work, one for simulation and one for the physical experiments. The simulation master device is a 2 DoF rigid-link robot composed of two revolute

joints. This device can be described by the values $q_m = [\theta_1\ \theta_2]^{\mathrm{T}}$. The physical master device, further described in Section 2.4 and Chapter 4, is a 9 DoF continuum device kinematically indentical to the OctArm. The main reason for two different master devices was to show end-effector convergence of a master device in simulation using traditional control techniques and to simplify the setup of the physical experiments.

2.1.1 Kinematic Model

The kinematic models of the master and slave systems are given by:

$$x_i(t) \triangleq f(q_i) \tag{2.1}$$

where $x_i \in \mathbb{R}^{n_i}$ is the position in the task space and $f(q_i) \in \mathbb{R}^{n_i}$ denotes the forward kinematics of the manipulator. The first and second derivatives with respect to time are:

$$\dot{x_i}(t) = J_i \dot{q_i} \tag{2.2}$$

$$\ddot{x_i}(t) = \dot{J_i}\dot{q_i} + J_i\ddot{q_i} \tag{2.3}$$

where $J_1 \in \mathbb{R}^{n_1 \times n_1}$ is the Jacobian of the master system. The development of the Jacobian for the slave system can be found in [35].

The homogeneous transformation matrix describing the coordinate and orientation transformation to the base plane of a planar, single section continuum [14] robot is given by equation (2.4).

$$H = \begin{bmatrix} \cos(s_i\kappa_i) & -\sin(s_i\kappa_i) & 0 & \frac{\cos(s_i\kappa_i)-1}{\kappa_i} \\ \sin(s_i\kappa_i) & \cos(s_i\kappa_i) & 0 & \frac{\sin(s_i\kappa_i)}{\kappa_i} \\ 0 & 0 & 1 & 0 \\ 0 & 0 & 0 & 1 \end{bmatrix} \tag{2.4}$$

The first three columns contain information concerning change of coordinate frames from the end effector to the base frame. The right most column contains the cartesian coordinates of the end point of a given continuum section dependent on the values $s(t)$ and $\kappa(t)$. This transformation is used to

determine desirable end-effector locations for both the master and slave systems in simulations by inputing values for $s(t)$ and $\kappa(t)$ and evaluating the cartesian values obtained from the matrix.

2.1.2 Dynamic Model

The dynamic model of the planar slave device, detailed in [21], is of the form:

$$M(q)\ddot{q} + C(q,\dot{q})\dot{q} = \tau \tag{2.5}$$

where $M(q) \in \mathbb{R}^{6\times6}$ is the inertia matrix, $C(q,\dot{q}) \in \mathbb{R}^{6\times6}$ is the Cetripetal-Coriolis matrix, and $\tau \in \mathbb{R}^6$ is the control input for the planar continuum manipulator. The variables $\ddot{q}$, $\dot{q}$, and q are the acceleration, velocity, and position of the system. The matrix $M(q)$ is symmetric and positive definite and satisfies the following inequalities [43]

$$m_{1i}\|\xi\|^2 \leq \xi^T M_i(\cdot)\xi \leq m_{2i}\|\xi\|^2, \qquad \forall \xi \in \mathbb{R}^6 \tag{2.6}$$

where m_{1i}, $m_{2i} \in \mathbb{R}$ are positive constants and $\|\cdot\|$ implies the standard Euclidean norm. Further, the matrix $(\dot{M} - 2C)$ is skew-symmetric such that:

$$\xi^T(\dot{M} - 2C)\xi = 0. \qquad \forall \xi \in \mathbb{R}^6 \tag{2.7}$$

These relationships are exploited when developing the controller.

2.2 Control Design

The goal of the control design is to cause asymptotic tracking convergence between the end effector position of the master and slave systems. Given the simplicity of the two-dimensional (2D) master system, a PD controller is adequate to cause asymptotic convergence to its desired position. For the continuum slave, the use of a previously developed Jacobian-based kinematic controller, seen in [14], does eventually allow the end-effector to asymptotically reach the desired position, as simulated in Figure 2.5, but does not enable the timely convergence to the solution required for effective use of the continuum robot. Therefore, it was anticipated that a nonlinear control strategy would be better suited for the control of this inherently nonlinear system.

In order to simplify the modeling, some assumptions were made that further impact the design of the control law. These assumptions are:

1. The slave system is operating on a plane parallel to the ground, negating the impact of gravity on the dynamic model.

2. The underlying surface on which the slave system moves is passive and frictionless.

3. The master device is capable of controlling all the degrees-of-freedom available to the slave system.

4. The slave system does not grasp objects, or otherwise contact the environment, to change its mass or dynamic properties.

2.2.1 Control Synthesis

In order to create the nonlinear controller, first a Lyapunov function was defined for the slave system:

$$V(t) \triangleq \frac{1}{2} s^T M s \tag{2.8}$$

where

$$s(t) = \begin{bmatrix} \dot{\tilde{q}_1} + \lambda \tilde{q_1} \\ \dot{\tilde{q}_2} + \lambda \tilde{q_2} \\ \dot{\tilde{q}_3} + \lambda \tilde{q_3} \\ \dot{\tilde{q}_4} + \lambda \tilde{q_4} \\ \dot{\tilde{q}_5} + \lambda \tilde{q_5} \\ \dot{\tilde{q}_6} + \lambda \tilde{q_6} \end{bmatrix}, \tag{2.9}$$

where the coefficient λ is a positive, real-valued constant. The values $\dot{\tilde{q}_i}$ and $\tilde{q_i}$ are velocity and position errors between the slave system and the desired position defined as:

$$\dot{\tilde{q}_i} = \dot{q_i} - \dot{q_{di}}, \tag{2.10}$$

$$\tilde{q_i} = q_i - q_{di}, \tag{2.11}$$

where q_{di} and $\dot{q_{di}}$ are the desired position and velocity of the ith control parameter for the slave system. Further, we find the time derivative of the Lyapunov function as:

$$\dot{V} = \frac{1}{2}s^T M\dot{s} + \frac{1}{2}\dot{s}^T Ms + \frac{1}{2}s^T \dot{M}s \tag{2.12}$$

$$= s^T M\dot{s} + \frac{1}{2}s^T \dot{M}s. \tag{2.13}$$

Here $\dot{s}(t)$ is

$$\dot{s}(t) = \begin{bmatrix} \ddot{\tilde{q}_1} + \lambda\dot{\tilde{q}_1} \\ \ddot{\tilde{q}_2} + \lambda\dot{\tilde{q}_2} \\ \ddot{\tilde{q}_3} + \lambda\dot{\tilde{q}_3} \\ \ddot{\tilde{q}_4} + \lambda\dot{\tilde{q}_4} \\ \ddot{\tilde{q}_5} + \lambda\dot{\tilde{q}_5} \\ \ddot{\tilde{q}_6} + \lambda\dot{\tilde{q}_6} \end{bmatrix}. \tag{2.14}$$

Using the expanded definition for $\dot{s}$:

$$\dot{s} \triangleq \ddot{q} - \ddot{q_d} + \lambda\dot{\tilde{q}}, \tag{2.15}$$

it is rearranged to become

$$\dot{s} = \ddot{q} - \ddot{q_r}, \tag{2.16}$$

defining the variable $\ddot{q_r} \triangleq \ddot{q_d}$ - $\lambda\dot{\tilde{q}}$. By substituting equation (2.16) into the derivative of the Lyapunov function in Equation (2.12), we obtain:

$$\dot{V} = s^T M(\ddot{q} - \ddot{q_r}) + \frac{1}{2}s^T \dot{M}s \tag{2.17}$$

$$= s^T(\tau - M\ddot{q_r} - C\dot{q}) + \frac{1}{2}s^T \dot{M}s \tag{2.18}$$

Finally, using the definition $\dot{q} \triangleq s + \dot{q_r}$ and substituting into equation (2.17), we have the

derivative of the Lyapunov function as:

$$\dot{V} = s^T(\tau - M\ddot{q_r} - C(s + \dot{q_r})) + \frac{1}{2}s^T\dot{M}s \tag{2.19}$$

$$= s^T(\tau - M\ddot{q_r} - C\dot{q_r}) + \frac{1}{2}s^T(\dot{M} - 2C)s \tag{2.20}$$

$$= s^T(\tau - M\ddot{q_r} - C\dot{q_r}) \tag{2.21}$$

The term $\frac{1}{2}s^T(\dot{M} - 2C)s$ is zero due to the skew-symmetric property of $(\dot{M} - 2C)$ given in equation 2.7.

In traditional adaptive control, the results from equation (2.19) can be used to create an estimate of unknown manipulator variables, such as mass at the end-effector. However, in this research, all parameters are assumed known due to the passive environment and Assumption 4 that the slave manipulator will not be grasping objects that alter the system's mass. As such, we simply need to design a control input that can ensure asymptotic tracking convergence and provide stability. Thus, the following control law is proposed:

$$\tau = M(\ddot{q_d} - 2\lambda\dot{\tilde{q}} + \lambda^2\tilde{q}) + C\dot{q_r}. \in \mathbb{R}^6 \tag{2.22}$$

2.2.2 Stability Result

Before implementing the control law, the stability of the system needs to be determined. First, substituting equation (2.22) into equation (2.19) for τ yields:

$$\dot{V} = s^T(M\ddot{q_d} - 2\lambda M\dot{\tilde{q}} + \lambda^2 M\tilde{q} + C\dot{q_r} - M\ddot{q_r} - C\dot{q_r}) \tag{2.23}$$

$$= s^T M(-\lambda\dot{\tilde{q}} - \lambda^2\tilde{q}) \tag{2.24}$$

$$= -s^T(\lambda M)s \tag{2.25}$$

As mentioned previously, M is a positive definite matrix and λ is a positive constant, making the term $-s^T(\lambda M)s$ negative-definite. Coupled with the positive-definite nature of the Lyapunov function in equation (2.8) the solution is determined to be asympototically stable in the sense of Lyapunov.

2.3 Controller Simulation

Simulations were run to test the effectiveness of the control law. A simulated dynamic model of the OctArm in planar motion was first used to test the convergence of the Jacobian-controlled OctArm [14], [44], [45], [21] and then the convergence of the slave system using the nonlinear control input. In order to determine an end-effector position achievable by the OctArm, the desired position for simulation was determined by selecting a random OctArm configuration and then using the OctArm forward kinematics to calculate the resulting end-effector location. For the simulations reported below, the desired slave configuration was set to be:

$$q_d = \begin{bmatrix} s_1 \\ s_2 \\ s_3 \\ \kappa_1 \\ \kappa_2 \\ \kappa_3 \end{bmatrix} = \begin{bmatrix} 0.3233 & m \\ 0.5000 & m \\ 0.4250 & m \\ 0.040 & m^{-1} \\ -0.020 & m^{-1} \\ 0.052 & m^{-1} \end{bmatrix}$$

Using the OctArm forward kinematics for a three section continuum robot, the desired end-effector location for the sbove OctArm configuration was determined to be:

$$x = \begin{bmatrix} z \\ x \end{bmatrix} = \begin{bmatrix} 1.248 & m \\ -0.012 & m \end{bmatrix}$$

where $z \in \mathbb{R}$ and $x \in \mathbb{R}$ are the coordinates for the base frame, illustrated as z_0 and x_0 in Figure 2.3.

The tracking error of the master device to the desired position can be seen in Figure 2.4, where asymptotic convergence is achieved through the use of the inverse Jacobian. Figure 2.5 depicts the error tracking between the master and slave device when relying on the inverse Jacobian of the slave system to control its end-effector's location. These errors do eventually converge to the master's end-effector location, but convergence is not smooth and takes an a priori unpredictable amount of time.

Figures 2.6, 2.7, 2.8, and 2.9 depict the corresponding tracking errors between the master

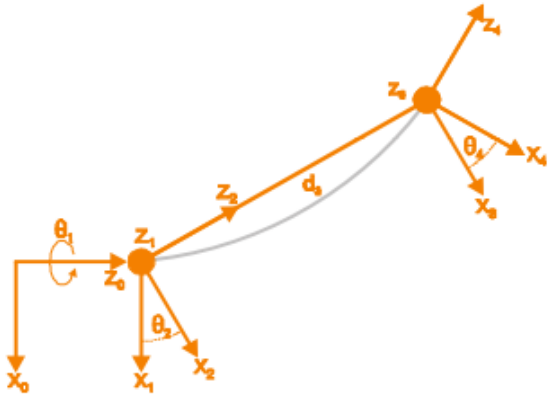

Figure 2.3: OctArm Coordinate System

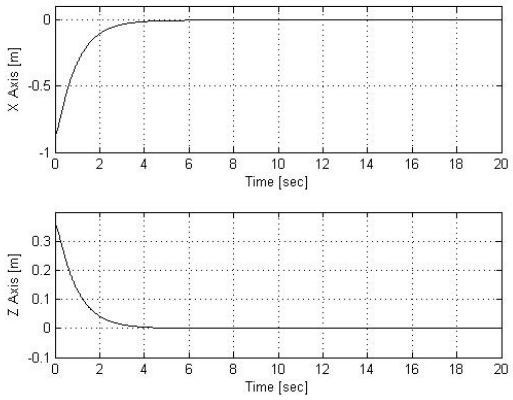

Figure 2.4: Master System Tracking Error

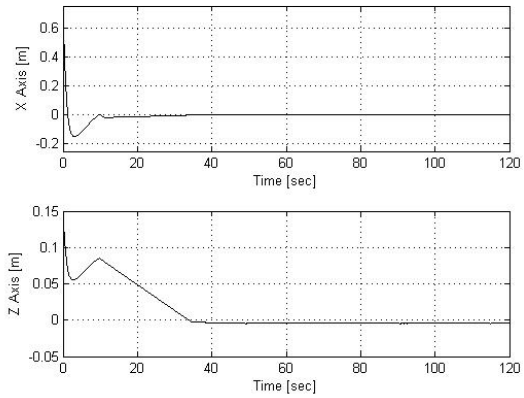

Figure 2.5: Jacobian Controlled Slave System Tracking Error

and slave system with the implementation of the nonlinear controller for different values of λ. The plot of the slave error in Figure 2.8 is magnified in order to observe the oscillations occuring in the tracking error of the Z coordinate. As can be seen, the time of convergence and the oscillation of the error decreases as the value of λ increases. A value of $\lambda = 25$ was found to produce an asymptotically converging tracking error while also eliminating oscillations seen in lower values of λ.

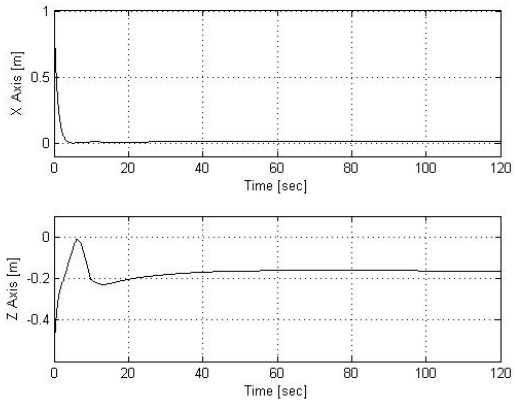

Figure 2.6: Slave System Tracking Error, λ=1

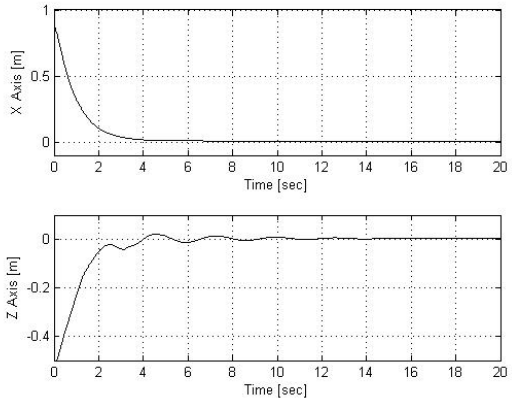

Figure 2.7: Slave System Tracking Error, $\lambda = 5$

In order to simulate the reality of a noisy system feedback in an actual system, an additional simulation was performed with Additive Gaussian white noise introduced into the feedback loop of the system. The Signal to Noise Ratio (SNR) of the Gaussian input was 30 dB, the impact of which can be seen in Figure 2.10. The end-effector tracking error can still be observed asymptotically converging to zero despite the noise added to the system.

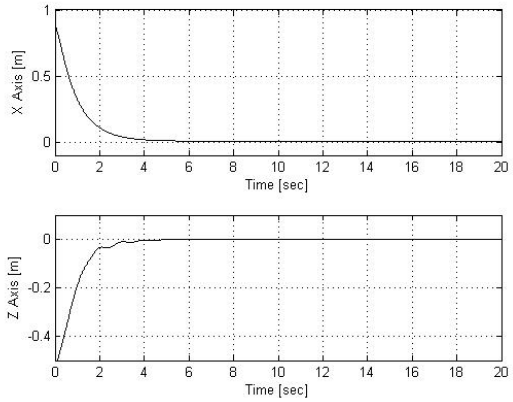

Figure 2.8: Slave System Tracking Error, $\lambda = 15$

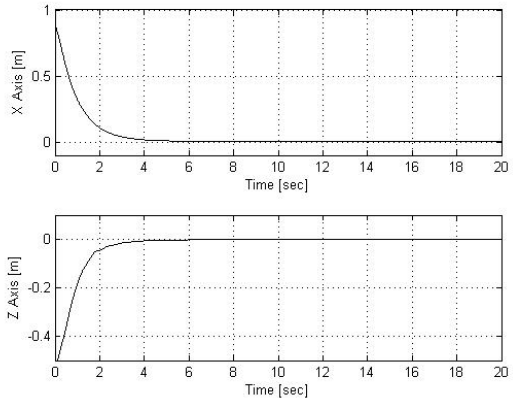

Figure 2.9: Slave System Tracking Error, $\lambda = 25$

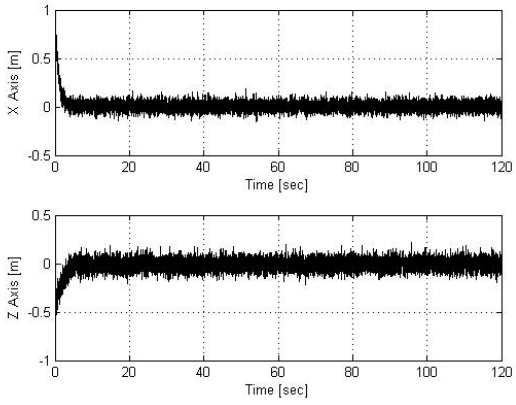

Figure 2.10: System Response with added White Gaussian Noise, SNR = 30 dB

2.4 Experimental Implementation

In order to validate the controller on a real continuum manipulator, experiments were conducted using the OctArm. The input device used was a 9 DoF continuum master device, described in Chapter 4. The master device is kinematically similar to the OctArm, comprised of three sections described by $s(t)$, $\kappa(t)$, and $\phi(t)$. In these experiments, only the arc length (s) and curvature (κ) values determined by the master device were used. All three sections of the OctArm were programmed to curve in the same planar direction.

The nonlinear controller was implemented in Matlab/Simulink [46]. A pair of Quanser Q8 data acquistion boards [47] were used to recieve the desired configuration set by the master device and output the values calculated by the nonlinear controller. The kinematic values determined by the master device were used as a set point within the Simulink model similar to the set point used in the simulations in Section 2.3.

There were 5 configurations chosen to highlight the effectiveness of the nonlinear controller. These were as follows:

1. No extension or curvature for any section.
2. Base section extended and curved.
3. Middle section extended and curved.
4. Tip section extended and curved.
5. All sections extended and curved.

The specific kinematic values set by the master device for each of the configurations are listed in Table 2.1.

Parameter	**Config 1**	**Config 2**	**Config 3**	**Config 4**	**Config 5**
s_{base} [m]	0.3234	0.3445	0.3233	0.3233	0.3437
s_{mid} [m]	0.3140	0.3140	0.3496	0.3140	0.3386
s_{tip} [m]	0.3387	0.3387	0.3387	0.3791	0.3623
κ_{base} [m^{-1}]	0.0012	0.0178	0.0012	0.0012	0.0160
κ_{mid} [m^{-1}]	0.0015	0.0083	0.0392	0.0015	0.0445
κ_{tip} [m^{-1}]	0.0047	0.0047	0.0047	0.0378	0.0296

Table 2.1: Kinematic Values for Experimental OctArm Configurations

For comparison, the same configurations were used in an open-loop control scheme of the OctArm. The following figures display both the end-effector error and tracking data for each con-

figuration from both the open loop and nonlinear closed loop controller. The tracking plots display the paths traveled by the ends of the base, middle, and tip sections of the slave device. These paths are colored cyan, green, and red, respectively. Also displayed are the desired set points of the base, middle, and tip section given by the master device. These appear as blue, dark green, and maroon stars. A black triangle marks the beginning of the base section for both the master and slave device and a black star designates the final end-effector position for the slave device.

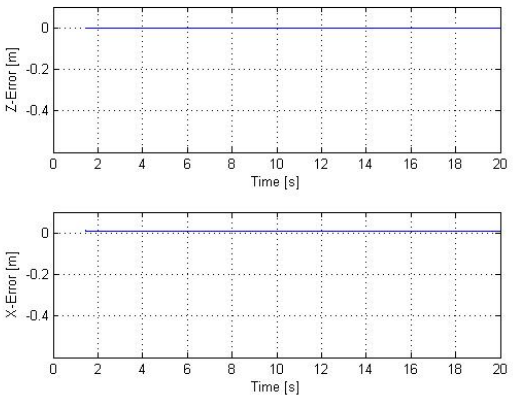

(a) Nonlinear End-Effector Error

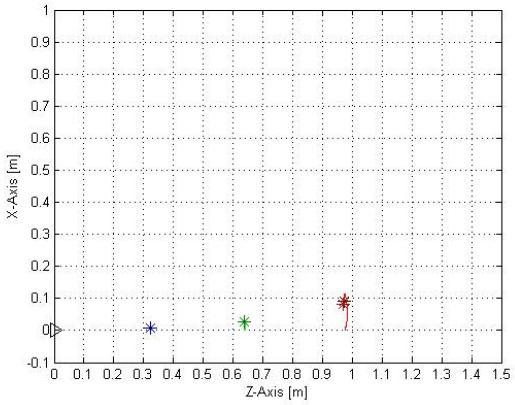

(b) Nonlinear Tracking Data

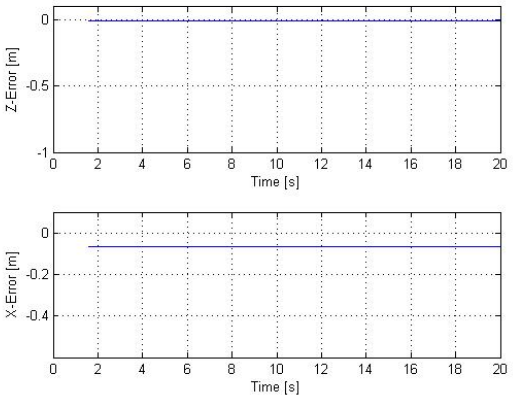

(c) Open Loop End-Effector Error

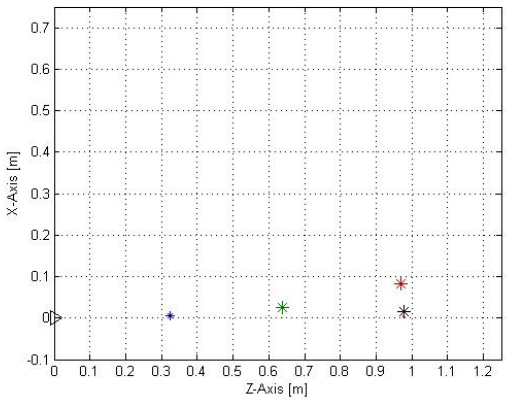

(d) Open Loop Tracking Data

Figure 2.11: Straight Configuration Tracking and Error Data

2.5 Discussion

The goal of this work was to develop a nonlinear controller for the teleoperation of a 6 Degree-of-Freedom continuum robot restricted to motion in a single plane. The desired outcome

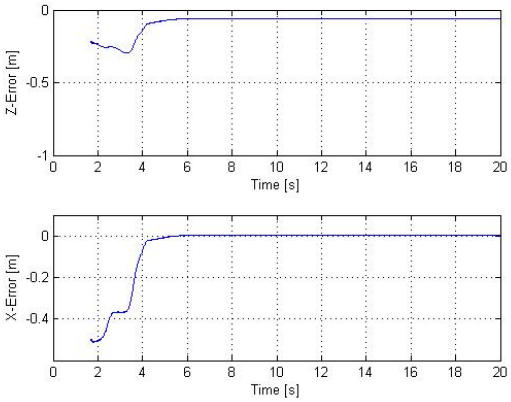

(a) Nonlinear End-Effector Error

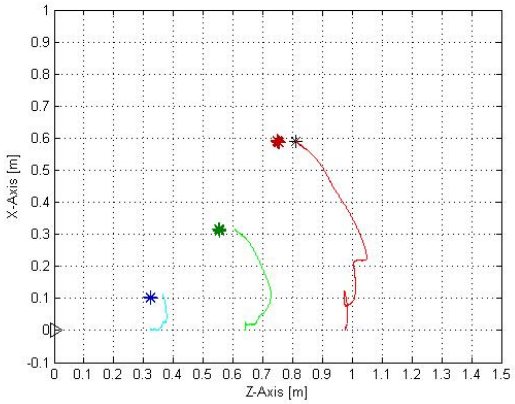

(b) Nonlinear Tracking Data

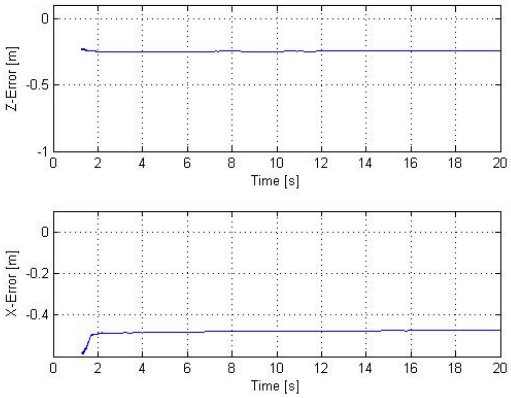

(c) Open Loop End-Effector Error

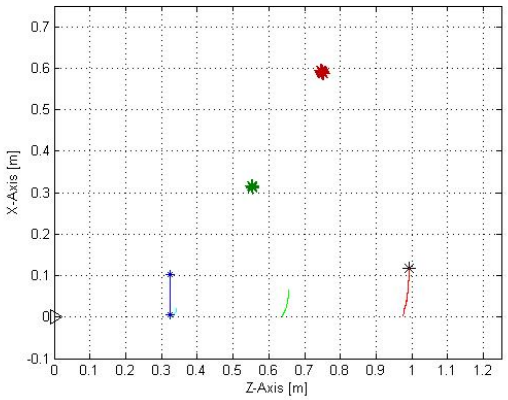

(d) Open Loop Tracking Data

Figure 2.12: Curving Base Section Configuration Tracking and Error Data

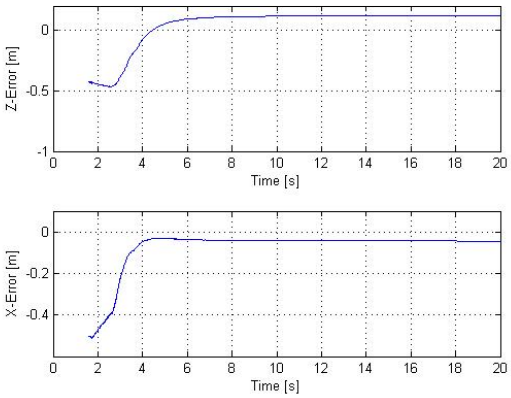

(a) Nonlinear End-Effector Error

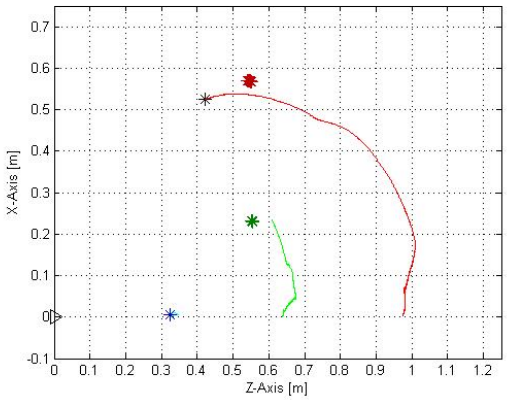

(b) Nonlinear Tracking Data

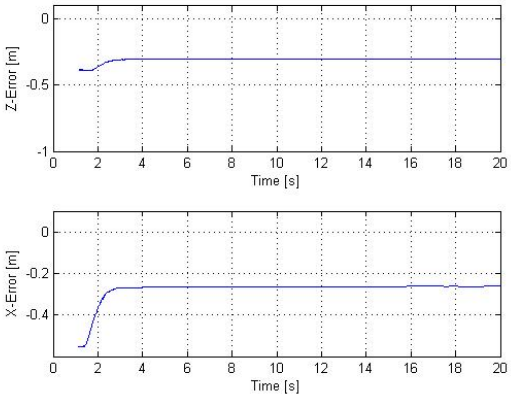

(c) Open Loop End-Effector Error

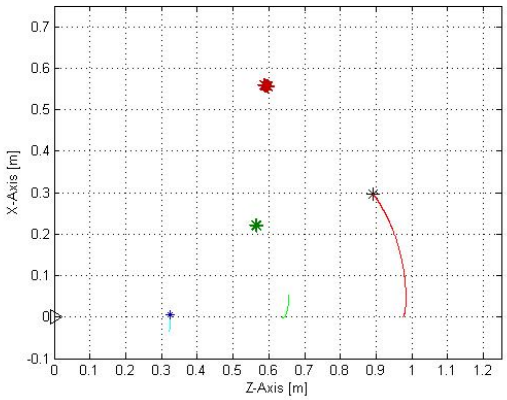

(d) Open Loop Tracking Data

Figure 2.13: Curving Middle Section Configuration Tracking and Error Data

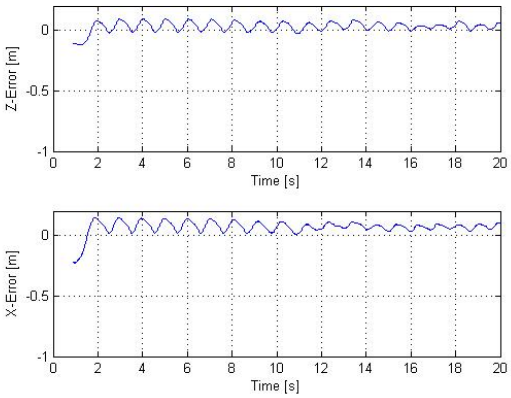

(a) Nonlinear End-Effector Error

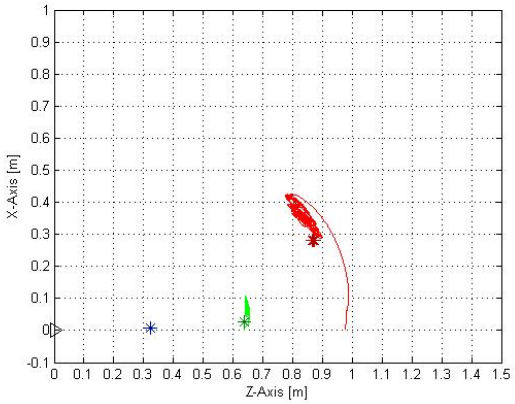

(b) Nonlinear Tracking Data

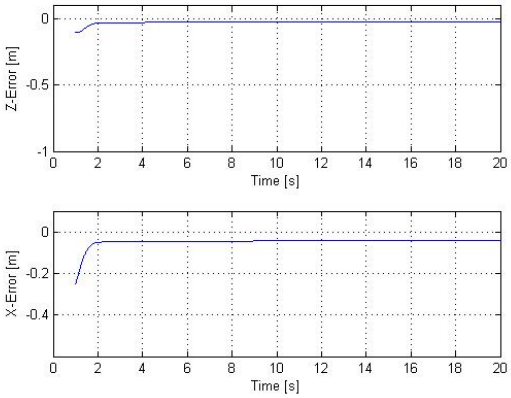

(c) Open Loop End-Effector Error

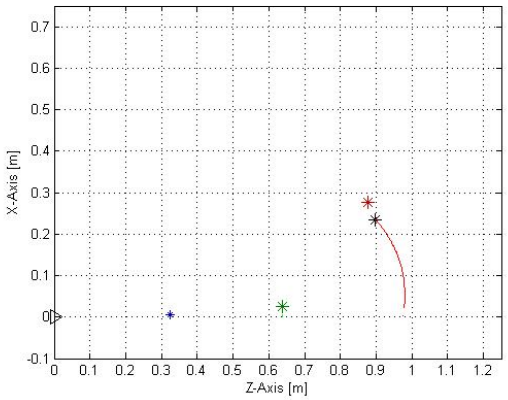

(d) Open Loop Tracking Data

Figure 2.14: Curving Tip Section Configuration Tracking and Error Data

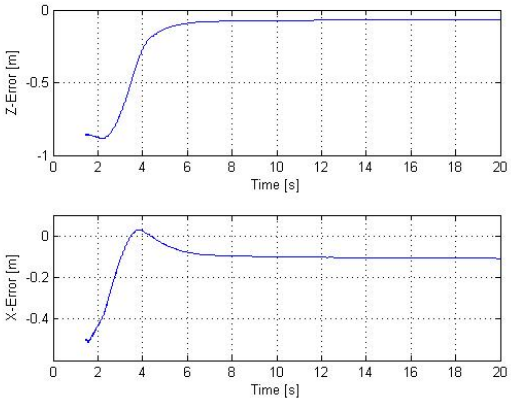

(a) Nonlinear End-Effector Error

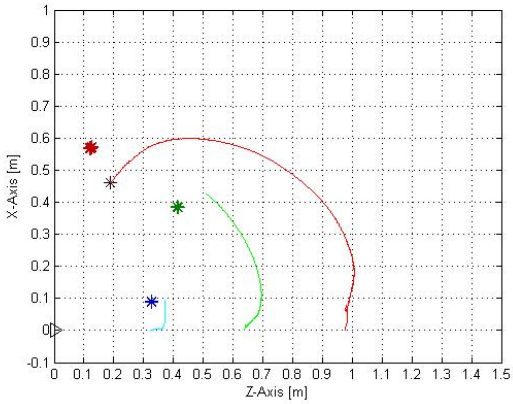

(b) Nonlinear Tracking Data

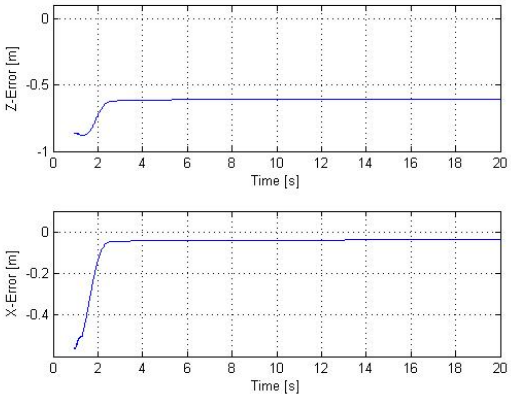

(c) Open Loop End-Effector Error

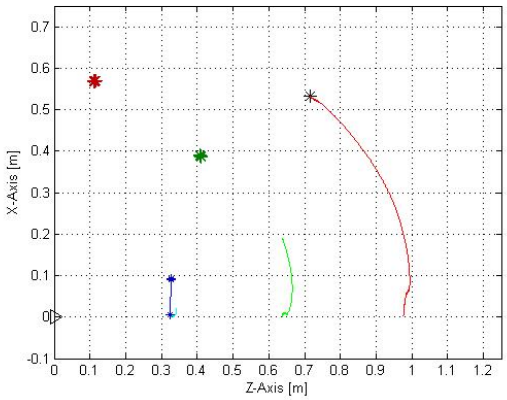

(d) Open Loop Tracking Data

Figure 2.15: All Sections Curving Configuration Tracking and Error Data

was to create asymptotic convergence between the location of the end-effector of the master and slave system. Initially, an adaptive control scheme was to be devised to control the slave system. However, after developing the Lyapunov function and determining the needs of the controller, it became apparent that adaptive control was not necessary due to the assumption of no uncertainties in either the model or the passive environment. Instead, a control law similar to that seen in typical adaptive control was used.

2.5.1 Simulation Results

The developed control law succesfully resulted in asymptotic tracking convergence between the master and slave system in simulation. In order to remain true to the system that the simulation models, it was important to choose end-effector positions obtainable by the physical OctArm manipulator and initial conditions that were within the operating range of the system.

As seen in the simulation results, Figures 2.6-2.9, an increase in the value of λ greatly influenced the accuracy and rate of convergence of the slave system. Small values of λ ($\lambda \leq 1$) caused the end-effector to over-shoot the desired position and resulted in either oscillating or constant error from the desired position. Larger values of λ ($\lambda > 1$) resulted in ideal asymptotic convergence, though moderate values of λ still produced small amounts of oscillation in the approach to zero-tracking error. Additionally, the slave system was still able to asymptotically converge to the solution despite the presence of Gaussian white noise in the system feedback loop.

2.5.2 Experimental Results

During the implementation of the nonlinear controller on the OctArm, multiple considerations were made when obtaining and analyzing the results. Most notable was the need to use a vector of varying λ values for each configuration in order to critically-damp the system response. During simulation, a single λ value for all 6 DoF was adequate for end-effector convergence. In experimentation, a single λ value assigned to the entire OctArm, or even a single section, produced an oscillatory response. Therefore, a vector of 6-λ values, one for each DoF, was implemented. The λ values used to produce the results in Section 2.4 varied for each configuration. These values are listed in Table 2.2.

The error and tracking plots in Section 2.4 reveal steady state errors in end-effector location

Parameter	Config 1	Config 2	Config 3	Config 4	Config 5
s_{base}	85	60	200	600	60
s_{mid}	85	200	380	300	60
s_{tip}	85	200	120	700	60
κ_{base}	85	450	200	1000	550
κ_{mid}	85	200	450	700	600
κ_{tip}	85	200	160	1500	650

Table 2.2: λ Values Corresponding to Experimental Configurations

and section end point locations. These errors can be attributed to a multitude of factors such as imperfections in system feedback, unmodeled friction, and physical limitations associated with continuum systems.

In order to evaluate potential error in system feedback and state estimation, the location of the OctArm end-effector was manually measured using a grid located in the plane of motion of the OctArm. The error between the manual measurements and state estimate values are located in Table 2.3. In configuration 4, the curving of the tip section, the error between the manual measurement and the state estimate at the end-effector location could not be captured due to the oscillations seen in Figure 2.14a.

Parameter	Z-Error	X-Error
Config 1	0.08	0.07
Config 2	0.02	0.09
Config 3	0.03	0.12
Config 4		
Config 5	0.01	0.10

Table 2.3: State Estimation Error [m]

The oscillations seen in Figure 2.14 are the result of underdamping λ values. Further testing of these values should yield a desirable end-effector convergence. While the currently reported result is not ideal, it highlights the impact of the λ values and shows oscillations occuring near or around zero error for both coordinates.

2.5.3 Research Impact

Further consideration can be given to implementing the developed control law for real-time tracking between master and slave devices instead of set point-convergence. This will include the

need to dynamically alter λ values during runtime. One possible solution for this is the implementation of a Kalman filter or similar tool to update λ depending on system error.

While the implemented control law performs as desired, there is still the desire to develop a truly adaptive control law for the control of continuum systems. Future work will examine the introduction of uncertainties into the models and environment, such as obstacles and objects to manipulate, as well as friction.

Additionally, there is the need to expand the control of a continuum system to space outside of the plane. This requires the development of a spatial dynamic model capable of modeling all of the degrees-of-freedom available to a three-section continuum robot. Once developed, nonlinear controllers such as the one examined in this chapter can be updated to address such a model.

Chapter 3

New Results in Teleoperation of Continuum Robots

Teleoperation has traditionally been, and remains, a key enabling element in implementation of many robotic systems, including continuum systems. To the best of the author's knowledge, only one work focusing on teleoperation modalities for continuum robots [34] based on using joysticks as input devices, has been reported in the literature prior to this work. In this chapter, we consider and demonstrate the teleoperation of continuum robots using rigid-link manipulators as input devices. The key innovation was to exploit the higher degrees of freedom (relative to conventional joysticks) of the rigid-link manipulators, to more intuitively map their movements to those of continuum robots.

3.1 The System

Driven by the inherent difficulty in understanding the operation of continuum robots, we sought to use a non-traditional approach to continuum robot control, using a non-redundant, rigid-link robotic arm as a teleoperative input device. The design of this experiment merges the two distinct topologies of rigid-link and continuum robotics with the intent of creating an intuitive relation that allows users to control continuum robots using rigid-link systems. This scheme gives the user physical control of a widely available system type with anthropomorphic kinematics in order to manipulate a more specialized device with more complex and less intuitive kinematics.

3.1.1 Continuum Robot Manipulator

In this study, the continuum system used was the OctArm [42], detailed in Chapter 2. The OctArm was operated in both planar and three dimensional space, resulting in 6 and 9 DoF parameters to be teleoperated.

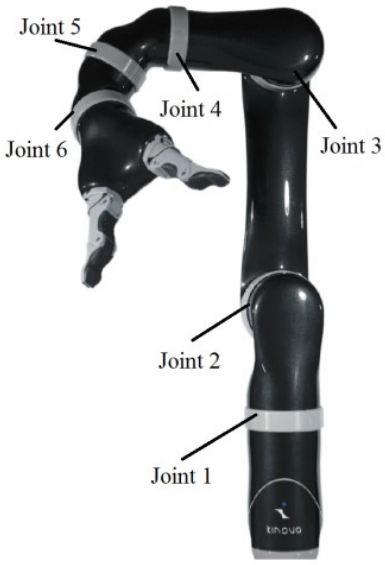

Figure 3.1: The 6 Degree-of-Freedom Kinova Mico Research Arm

3.1.2 Rigid Link Robot Controller

As our chosen teleoperative input device, we used a Kinova Mico Research Arm [48]: a kinematically non-redundant, rigid link arm with 6 DoF, shown in Figure 3.1. The Mico Arm was chosen because it is representative of the large range of anthropomorphic robotic arms and its size allows for easy manipulation by a human user. During experiments, the Mico Arm was placed in "float" mode, which allowed the user to manipulate the arm freely while the robot automatically compensated for gravity at each joint. Joints 2 and 3 have physically limited rotation (Joint 2 rotates between 35 and 325 degrees, Joint 3 is limited to rotation between 50 and 310 degrees as designated by the Mico Arm joint limit). The Mico Arm also features a gripper, but this element was not required in this study. The output of the Mico Arm in this study was a temporal series of joint angles produced by the 6 revolute joints to be mapped to the OctArm.

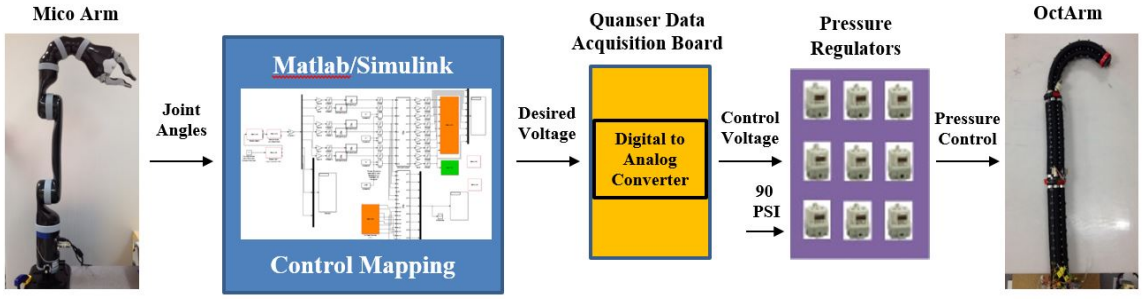

Figure 3.2: Teleoperative Control Block Diagram

3.1.3 Teleoperative Control

Several schemes were devised and tested in an attempt to learn the most intuitive control for the OctArm. Figure 3.2 depicts the control layout from the user through the Mico Arm and mapping software, and finally to the OctArm. As indicated, each test in the experiment can be broken into the following four steps:

Step 1: The user physically manipulated the Mico Arm by rotating any of the six available joints. Several joints could be manipulated at once or each joint could be operated independently.

Step 2: While the user manipulated the Mico Arm, the Kinova control software continually read each joint angle serially via a wired USB connection. The joint values then passed internally via a network socket to a Simulink model that controlled the OctArm.

Step 3: Within the Simulink model, a mapping designated how each of the Mico Arm joints was mapped to the movement of the OctArm. Using the 6 joint angles from the Mico, the model passed the values through function blocks that converted the joint angles into a combination of $s(t)$, $\kappa(t)$, and $\phi(t)$ values for each section of the OctArm. These mappings, and their effectiveness in providing intuitive teleoperation of the OctArm, are the focus of this chapter and are detailed further in Section 3.2.

Step 4: Once the 9 OctArm DoFs were calculated, they passed through another Simulink function block that calculates the necessary lengths for each actuator muscle within the different sections of the OctArm and the necessary pneumatic pressure to acquire each length. The individual pneumatic pressures were passed to the corresponding pressure regulators as analog control voltages through the use of a Quanser data acquisition board [47]. These pressures caused the OctArm to assume the configuration designated by the Mico Arm joint angles.

Mico Joint	P1	P2	P3	P4
1	$\kappa(t)_{Base}$	$\kappa(t)_{Base}$	$s(t)_{Base}$	$s(t)_{Base}$
2	$s(t)_{Base}$	$\kappa(t)_{Mid}$	$s(t)_{Mid}$	$\kappa(t)_{Base}$
3	$\kappa(t)_{Mid}$	$\kappa(t)_{Tip}$	$s(t)_{Tip}$	$s(t)_{Mid}$
4	$s(t)_{Mid}$	$s(t)_{Base}$	$\kappa(t)_{Base}$	$\kappa(t)_{Mid}$
5	$\kappa(t)_{Tip}$	$s(t)_{Mid}$	$\kappa(t)_{Mid}$	$s(t)_{Tip}$
6	$s(t)_{Tip}$	$s(t)_{Tip}$	$\kappa(t)_{Tip}$	$\kappa(t)_{Tip}$

Table 3.1: Variable Mappings For Planar Motion

3.2 Input Mappings

As the focus of this part of the research was intuitive control of redundant continuum systems, it was important to develop multiple control mappings between the OctArm and Mico Arm that would be easily understood by users. For both the planar and spatial motion experiments described in this chapter it was important to maintain a consistent organization between the configuration of the OctArm and that of the Mico Arm when designing each mapping. This is why for all future references in this paper, the base of the OctArm was assigned to correspond to the base of the Mico Arm, or Joint 1, and the tip of the OctArm was related to the end effector of the Mico Arm, or Joint 6.

3.2.1 Planar Motion Mappings

The first series of experiments conducted in this study limited the OctArm to a single plane of motion, parallel to the ground. This limitation restricted the OctArm to 6 DoF ($s(t)$ and $\kappa(t)$ for each of the three sections). In addition to the 6 DoF, a binary version of $\phi(t)$ was available for each section. These values dictated whether the section curved left or right in the plane with respect to the end of the previous section. The values of $\phi(t)$ did not impact the user or influence the layout of the mappings. Thus the ratio of DoF became a 1-to-1 ratio between the Mico Arm and the OctArm. The planar mappings were developed to assign a single OctArm value, $s(t)$ or $\kappa(t)$, to each section of the OctArm while keeping the previously established orientation. The available values of $\phi(t)$ were controlled by the same joint of the Mico Arm as the $\kappa(t)$ value of the same OctArm section. There were 4 mappings developed for the planar experiments, as described in Table 3.1.

3.2.1.1 Planar Mapping 1 (P1)

Mapping P1 of the planar experiments explored the idea of having the Mico Arm divided into operational sections similar to the OctArm. In this particular scheme, Joint 1 and Joint 2 together control the Base section, Joint 3 and 4 control the Middle section, and finally Joint 5 and 6 control the Tip section. For all pairings, $\kappa(t)$ was controlled by the first joint and $s(t)$ was controlled by the second joint. The idea behind this scheme derived from the similarity in section assignment of the controller to the inherent section division of the OctArm manipulator.

3.2.1.2 Planar Mapping 2 (P2)

In mapping P2, instead of dividing the Mico Arm into sections according to OctArm section assignment, the joints were grouped by the OctArm variables available, $s(t)$ and $\kappa(t)$. Joints 1, 2, and 3 of the Mico Arm controlled the $\kappa(t)$ value for the Base, Middle, and Tip section, respectively. Similarly, Joints 4, 5, and 6 controlled $s(t)$ for each OctArm section in order from Base to Tip section. It was anticipated that P2 would receive the highest intuition rating due to the physical constraints of the Mico Arm. The limitations of Joints 2 and 3 gave the two joints natural midpoints (180 degrees) for the value of $\phi(t)$ to alternate between its two planar values per section. The midpoint for both joints was easily discernible because it resulted in a straight line connecting the segments on both sides of each joints. Thus, incorporating the physical design of the Mico Arm was thought to increase the intuition of this mapping.

3.2.1.3 Planar Mapping 3 (P3)

Mapping P3 was an adaptation of Mapping 2. In this mapping, the $s(t)$ values were assigned to Joints 1, 2, and 3. $\kappa(t)$ was controlled by Joints 4, 5, and 6. This mapping was expected to enable performance with some ease but not as intuitively as P2. The idea of having all $s(t)$ values and all $\kappa(t)$ values grouped together allows manipulation of shape using a small group of Mico joints, as opposed to the use of almost the entire Mico Arm as in P1.

3.2.1.4 Planar Mapping 4 (P4)

The final mapping, mapping P4, is an adaptation of P1. In this mapping, the order of $s(t)$ and $\kappa(t)$ per section assignment were reversed; $s(t)$ is the first joint in each grouping of two Mico

Mico Joint	S1	S2	S3
1	$s(t)_{Base}$, $\kappa(t)_{Base}$	$s(t)_{Base}$, $\kappa(t)_{Base}$	$\phi(t)_{Base}$
2	$\phi(t)_{Base}$	$s(t)_{Mid}$, $\kappa(t)_{Mid}$	$s(t)_{Base}$, $\kappa(t)_{Base}$
3	$s(t)_{Mid}$, $\kappa(t)_{Mid}$	$s(t)_{Tip}$, $\kappa(t)_{Tip}$	$s(t)_{Mid}$, $\kappa(t)_{Mid}$
4	$\phi(t)_{Mid}$	$\phi(t)_{Base}$	$\phi(t)_{Mid}$
5	$s(t)_{Tip}$, $\kappa(t)_{Tip}$	$\phi(t)_{Mid}$	$\phi(t)_{Tip}$
6	$\phi(t)_{Tip}$	$\phi(t)_{Tip}$	$s(t)_{Tip}$, $\kappa(t)_{Tip}$

Table 3.2: Variable Mappings For Spatial Motion

joints and $\kappa(t)$ is second. This mapping was expected to perform similarly to P1 in intuitiveness using the appeal of Mico sections to control OctArm sections.

3.2.2 Spatial Motion Mappings

The Spatial Motion experiments allowed the OctArm the full range of motion, creating a 6-to-9 DoF ratio between the Mico Arm and the OctArm. This presented a unique problem of obtaining multiple additional distinct signals from the joints of the Mico Arm in a consistent way that allows for intuitive control of the OctArm. In developing the spatial motion mappings, the values of $s(t)$ and $\kappa(t)$ were chosen to share a single joint as opposed to the $\kappa(t)$ and $\phi(t)$ relationship used in the planar experiments. $\phi(t)$ for each OctArm section was given its own Mico Arm joint because the range of $\phi(t)$ is 0 to 360 degrees of revolution, which gives a 1-to-1 relation to the revolute joint angles. Using the fact that the Mico Arm outputs joint angles, a procedure was devised through the use of sinusoids of two different frequencies in order to transform the joint angle into a range from 0 to 2 that was then scaled to the maximum and minimum $s(t)$ and $\kappa(t)$ values for each prescribed OctArm section. The values of $s(t)$ and $\kappa(t)$ were calculated using the following equations:

$$s(t) = s(t)_{min} + (s(t)_{max} - s(t)_{min})\frac{(\sin(4\theta_i) + 1)}{2} \tag{3.1}$$

$$\kappa(t) = \kappa(t)_{min} + (\kappa(t)_{max} - \kappa(t)_{min})\frac{(\sin(\theta_i) + 1)}{2} \tag{3.2}$$

where θ_i is the angle output of Joint i and $s(t)_{min}$, $s(t)_{max}$, $\kappa(t)_{min}$, and $\kappa(t)_{max}$ are the minimum and maximum values of $s(t)$ and $\kappa(t)$, respectively. Three mappings were developed using these techniques and equations. Table 3.2 summarizes the breakdown of each spatial mapping.

3.2.2.1 Spatial Mapping 1 (S1)

The first spatial motion mapping was an extension of Mappings P1 and P4 of the planar motion experiments. Joints 1 and 2 of the Mico Arm controlled the three values of the Base section of the OctArm, Joints 3 and 4 controlled the Middle section, and Joints 5 and 6 controlled the Tip section. Within the groupings, $s(t)$ and $\kappa(t)$ were assigned to the first joint and $\phi(t)$ to the second. This mapping was anticipated to be the least intuitive of the proposed solutions. The main reason for this prediction was the fact that $\phi(t)$ for the Base section was assigned to Joint 2 of the Mico Arm. This meant that a variable signifying the 360 degree rotation of the OctArm section in space was controlled by a joint that could only rotate 260 degrees. Thus, the Base OctArm section would not be able to continuously rotate to any direction.

3.2.2.2 Spatial Mapping 2 (S2)

Similar to S1, Mapping S2 was derived from the planar experiment mappings; in this instance mappings P2 and P3. The $s(t)$ and $\kappa(t)$ values were controlled by Joints 1, 2, and 3 and $\phi(t)$ was controlled by Joints 4, 5, and 6. Similar to the planar versions, S2 was predicted to perform with greater intuitiveness than S1. In the spatial motion of the OctArm, the two most important factors are the orientation and shape. Isolating $s(t)$ from $\kappa(t)$ was not critical due to the redundancy and availability of multiple solutions. S2 therefore isolates the two major factors into distinct groups, allowing the user to easily locate which group of factors they need, shape or orientation.

3.2.2.3 Spatial Mapping 3 (S3)

Mapping S3 was an alteration of S1 that was intended to correct for the discontinuity of $\phi(t)$ for the Base section. The Base section was still controlled by Joints 1 and 2, the Middle section by Joints 3 and 4, and the Tip section by Joints 5 and 6. The joint pairs controlling the Base section and Tip section had $\phi(t)$ controlled by the first joint and $s(t)$ and $\kappa(t)$ values controlled by the second joint. The Middle section differed by having $\phi(t)$ controlled by the second joint (Joint 4) and $s(t)$ and $\kappa(t)$ controlled by the first joint. This mapping ensured that each $\phi(t)$ was assigned to a revolute joint without physical limits. The anticipation of this mapping was that it would be more intuitive than S1 but still less intuitive than S2 because of the switch in OctArm variable control order.

3.3 Study Design

A study was designed to step participants through a series of tasks that increasingly evolved in complexity in order to develop a procedure for systematically evaluating the control of the OctArm. This procedure was created to test the full range of each mapping in Section 3.2 and to force the participants to use every joint of the Mico Arm to reach the solutions. The study comprised of two separate parts, planar and spatial motion manipulation. The overall study used a group of 15 participants to test the mappings; 7 tested planar teleoperation and 8 tested spatial teleoperation. Volunteer participants were recruited from among students and faculty of Clemson University, with a wide range of academic backgrounds and areas of study. Demographic details of the participants are given in Section 3.4.1.

3.3.1 Planar Motion Study Goals

The main focus of the planar experiments was the establishment of the baseline feasibility of using a rigid-link robotic arm as a viable, intuitive control device for a continuum robot. The use of outside participants was expected to give us insight into the following questions:

1. Can a rigid-link robot with a 1-to-1 DoF relation be reliably used to control a continuum robot in planar motion?

2. Is there an intuitive control mapping solution set that can be used by non-experts? If so, which of the developed mappings most fulfills this goal?

3. Is there an advantage to using such a teleoperative solution in controlling continuum robots over using a kinematically-similar controller?

3.3.2 Spatial Motion Study Goals

The Spatial Motion portion of this study took place after the conclusion of the planar experiments, which led to a development of new study questions and goals. The main goal of the spatial motion trials comprised an attempt to find the most intuitive and universal solution to the teleoperation of general 3D motions of continuum robots using the rigid-link system. The following research questions were developed for the spatial motion trials:

1. Can a non-redundant system adequately be used to control a kinematically-redundant continuum system?

2. Does robotic or gaming experience have an impact on intuitive use of such control mappings?

3. Is there a spatial motion mapping solution developed in this study that could be applicable to non-experts?

3.3.3 Study Setup

In the establishment of this study, it was important to create a consistent plan for the execution of experiments to be used for both the planar and spatial motion experiments. We ensured that the subjects received the same set of instructions in order to perform the assigned tasks, whether they were planar or in 3D space. Thus, each participant underwent the same three phases (detailed in the following subsections) for each of the available mappings:

1. Warm Up Phase
2. Task Phase
3. Evaluation Phase

In conjunction with the physical testing, participants were asked to complete a non-invasive and anonymous questionnaire that asked about video gaming experience, robotic experience, and field of academic study, which is included in Appendix A. For this, we obtained study approval from the Institutional Review Board (IRB) concerning the acquistion of participant information. At no point in the study were the mappings of the Mico Arm joints to the OctArm values disclosed to the participants in the study, the goal being to preserve the evaluation of intuitive control. Each volunteer in the study tested every mapping for either planar or spatial motion and the order in which mappings were tested was kept consistent for all participants. The order of testing was determined by the order in which the mappings were created.

Prior to the beginning of the experiment, each participant was given a brief introduction to the OctArm and Mico Arm which detailed what movements the participants could expect to see and what configurations both the Mico Arm and OctArm were capable of reaching. Next, the participants were instructed to manipulate the Mico Arm without the OctArm running in order to gauge the amount of force necessary to rotate each joint of the arm and understand the complete range of motion capable of the Mico Arm joints.

3.3.3.1 Warm Up Phase

The Warm Up Phase of the experiment was the first introduction of the participant to actually controlling the OctArm. For each mapping used, numbering either four for Planar or three for Spatial motion, in the experiment, the participant was given up to 5 minutes, to experiment with each joint of the Mico Arm and observe the corresponding reaction of the OctArm. During the warm up phase participants were allowed to write down observations or guesses at the layout of each mapping in order to help remember the order of Mico Arm joint assignments during the following phases of the experiment.

3.3.3.2 Task Phase

During the Task Phase, the participants were given a series of OctArm shapes to create or goals to achieve using the OctArm. In the Planar experiments, the participants were tasked to form four shapes, seen in Figure 3.3, each evolving in complexity of manipulation of both the OctArm and Mico Arm than the previous shape. The final task of the Planar experiment was to move the end of the Tip section to an X marked on the plane on which the OctArm rested during that portion of the study.

In the Spatial Motion study, participants were given three tasks for each mapping, depicted in Figure 3.4. The first task tested the user for control of $\phi(t)$ by having the participant orient each section of the OctArm so that they all curved into the same plane. The second task tested control of all 9 OctArm DoF by having the end-effector of the OctArm once again reach an X marked on a board placed close to the OctArm. This second task had several possible solutions, but the awareness of $s(t)$ and $\kappa(t)$ were important in having the end effector at the correct height. The final task tested for a relatively in-depth understanding of all 9 DoF. For this task, a marker was fixed to the end of the Tip Section of the OctArm. The participant was then tasked with drawing a straight, vertical line on the white board that contained the X from Task 2.

During the Task Phase, participants were offered coaching to complete tasks, for example advice about increasing the curvature of a particular OctArm section, without stating which joint of the Mico Arm they needed to manipulate to follow the council. Participants were video recorded performing the tasks to help analyze the approaches users took to problem solving with the OctArm. Additionally, during the Task Phase, participants were given a time limit to perform each task,

1^{st} Task: Return to Straight Line

2^{nd} Task: Curve Tip Section

3^{rd} Task: All Sections Curve in Single Direction

4^{th} Task: Alternate Directions of Curve

Figure 3.3: Orientation Based Tasks for Planar Motion Study

1^{st} Task: Planar Orientation of Sections

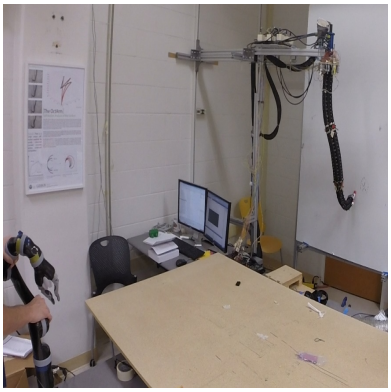

2^{nd} Task: Place End of OctArm to Target X

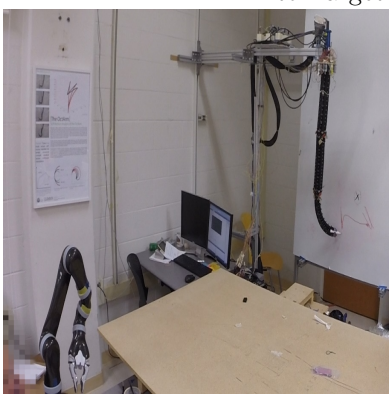

3^{rd} Task: Draw Vertical Line on Background

Figure 3.4: Task Phase of Spatial Motion Study

motivated by the idea that intuitive control should be quick to learn. This limit was 5 minutes for the planar motion tasks and 10 minutes for the spatial motion tasks. The Spatial Motion limit was set longer due to the redundancy of the OctArm and the presence of several solutions to each task.

3.3.3.3 Evaluation Phase

In the Evaluation Phase the participants completed a final questionnaire, available in Appendix A, at the conclusion of the experiment. For each mapping in the experiment, there were two questions. The first question requested participants give each mapping a rating, with the choices being: intuitive, usable, usable with practice, difficult to use, and unusable. The participants were then asked to evaluate how they believed the general public would perform while using each of the mappings, using the same scale from the first question. This question was formulated to gauge how participants rated their abilities to use the system in comparison to the general populace.

3.4 Experimental Results

The main evaluation criteria from this study falls into three categories. First, we analyzed the results from the questionnaire for both the planar and spatial motion experiments. This mode presents the most detailed evaluation of how participants viewed the control mappings. Secondly we analyzed the data regarding the completion of tasks within the time constraints; for a control scheme to be truly intuitive the user must be able to complete assigned tasks in a timely manner. The third catergory used for evaluation was the analysis of the correlation between user performance and video gaming or robotics background.

3.4.1 Questionnaire Results

This section summarizes all of the information collected in both the initial questionnaire and the evaluation of the mappings from each participant. The results are present for both the planar and spatial motion experiments.

The total number of participants for the study was 15; 7 were used in the planar motion study and 8 participated in the spatial motion experiments. There were 4 participants that took part in both the planar and spatial motion experiments. Of the 15 participants, 8 were male, 7 were female.

In the planar motion study, all 7 participants reported having little or no previous experience with robotics, only 2 were noted to have any experience at all. However, all participants but one in the planar study claimed to have video gaming experience, varying from one year up to 15 years. Four of the eight spatial motion participants reported having robotic experience and all reported having some level of video game experience. The ages of the participants ranged from 18 to 30 years of age, with the majority being between 18 and 21.

The results of the planar mapping evaluations are shown in Figure 3.5. The evaluations were scaled to range from 0 to 4, where 0 indicates an unusable control mapping and 4 indicates an intuitive control mapping between the Mico Arm and OctArm. Displayed in the table are the average ratings the participants gave based on their performance and how well they thought the general population would do with the control mappings. Additionally displayed is the standard deviation for each mapping. Figure 3.6 displays the corresponding information for the Spatial Motion experiments.

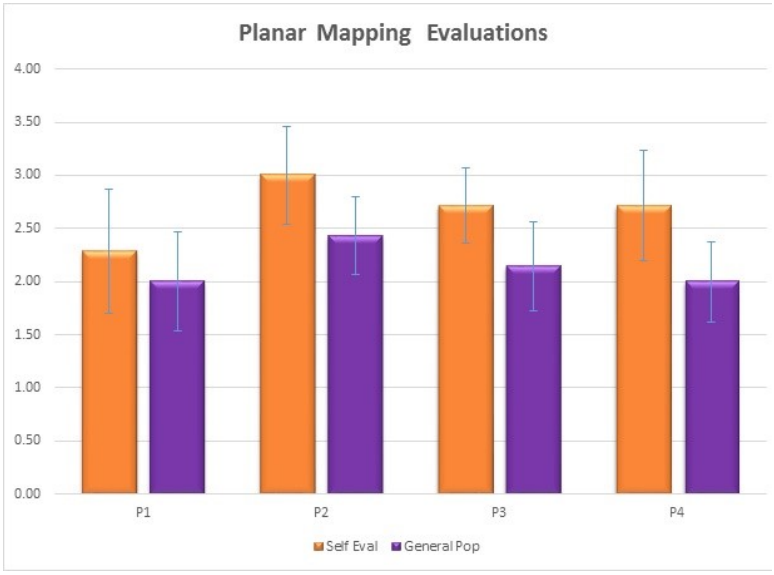

Figure 3.5: Average and Standard Deviation of Planar Mapping Evaluations

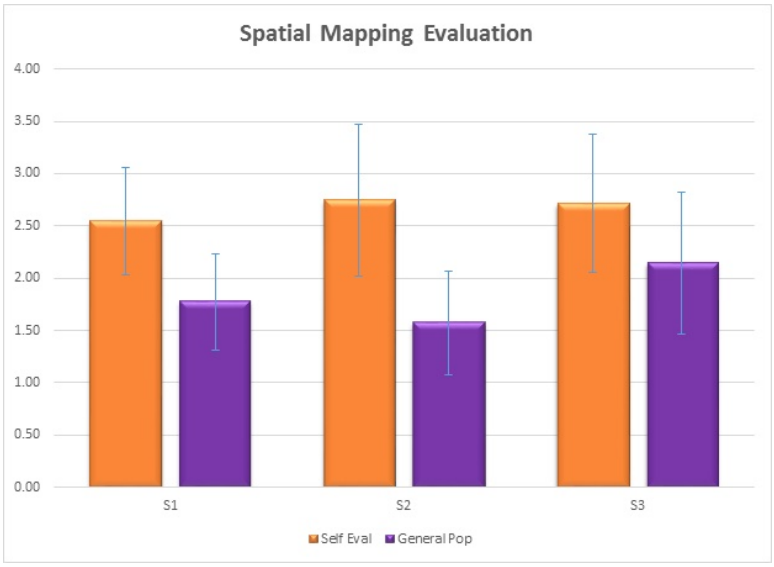

Figure 3.6: Average and Standard Deviation of Spatial Mapping Evaluations

In the planar experiments, mapping P2 received the highest rating for both Self Evaluation ($M = 3$, $SD = 0.92$) and General Population ($M = 2.43$, $SD = 0.73$). P3 and P4 in the planar experiments earned the same average Self Evaluation rating ($M = 2.71$) but P3 had a smaller deviation ($SD = 0.83$) than P4.

The results of the spatial motion questionnaires revealed mapping S2 to have the highest average for the Self Evaluation ($M = 2.74$, $SD = 1.46$) but S3 was rated to be better for the general population ($M = 2.14$, $SD = 1.36$).

3.4.2 Task Completion

In the planar experiments, nearly all participants were able to complete the 5 tasks for each of the 4 mappings. This part of the study had a 85.7% completion within the designated time limit. There was one participant that failed to complete each task for all 4 mappings in the allotted time. In the spatial motion experiments, some participants failed to complete all of the assigned tasks within the allotted time. Table 3.3 displays the completion percentage for each mapping and for each of the assigned tasks.

Task	**S1**	**S2**	**S3**
1	88 %	75 %	88 %
2	75 %	75 %	75 %
3	75 %	63 %	75 %

Table 3.3: Completion Percentage for Each Spatial Mapping

It can be seen that mapping S2, while receiving the highest Self Evaluation rating, had the lowest completion percentage of the 3 mappings. Mappings S1 and S3 were the most successful of the mappings, with equal completion for all 3 tasks.

3.5 Discussion

The operation of the system worked well enough for us to evaluate our initial goals. The majority of participants were able to complete the desired tasks, both in planar and spatial motion, well within the desired time. The teleoperative system did experience lag between the manipulation of the Mico Arm and the motion of the OctArm, this lag is an expected challenge when working with teleoperative control. In this study, the lag was primarily the result of signal filtering of the

Mico output in order to reduce noise produced by the serial communication of joint angles and did not significantly affect the user's ability or completion time.

3.5.1 Expected Results

In the overall study, our goal was to create an intuitive control mapping that allowed novice robot users to control a continuum robotic system with ease. In viewing the results from the planar experiments we achieved success in creating control mappings that nearly all participants could use to reliably control the OctArm. As predicted, mapping P2 had the most success in providing participants with intuitive control. However, the ratings P2 received from the participants were only marginally above those of both P3 and P4. In general, the fact that the remaining mappings were also rated as reasonably usable encourages the idea that, for the planar application of this system, rigid-link teleoperation of a continuum system is a viable solution, though not necessarily perfectly intuitive.

In the spatial motion experiments, the results of the study were less clear. Though some participants were highly successful in completing tasks and using the system, the evaluations received from participants were contradictory. Mapping S2 received the highest rating for self-evaluation but S3 was rated to be the easiest for use by the general public. S1 was the lowest in both categories, which aligned with our prediction. The combination of $s(t)$ and $\kappa(t)$ together created some challenges for participants because of the sensitivity of OctArm responses to the $s(t)$ value. In equation (3.1), which calculated $s(t)$ for each section, the choice to have $s(t)$ complete four cycles for one cycle of $\kappa(t)$ was meant to create several combinations of the two values, providing more possible configurations to the user. In the actual implementation, this coupling caused the sections of the OctArm to change length too quickly for some participants to find a precise solution in a short amount of time. One technical solution to this would be to reduce the frequency of the $s(t)$ cycle and test which ratio of $s(t)$ to $\kappa(t)$ cycle provides the best response.

3.5.2 Experience Impact

During the experiments and after analyzing the participant demographic, it appears that prior robotic experience or prior gaming experience had little to no impact on participants' intuitive ability to use the system. However, due to the small number of participants and the inability to

create two distinct groups of experienced and inexperienced volunteers, further testing would be required to make definitive claims with respect to this question.

3.5.3 Research Impact

The results of this study provides evidence that a rigid-link manipulator can be used as a viable master device in the teleoperation of continuum robots. However, the results of the surveys and completion percentages suggest that this form of master device may not be the most intuitive and easy to use device for such schemes. Resultant ongoing work (see next Chapter) considers the development and implementation of a kinematically similar master device capable of manipulating all available DoF in the slave device. More potential work could compare several potential master devices, such as the rigid-link arm reported in this chapter, the joystick referenced in [34], and future devices in order to determine which proves most intuitive to users.

Chapter 4

A Kinematically-Similar Master Device for Extensible Continuum Manipulators

As discussed in previous chapters, the teleoperation of continuum manipulators has seen a limited attempt at the intuitive and effective manipulation of continuum slave devices. One suggested solution [49] has been to develop a kinematically similar master device capable of directly mapping all DoF available to a continuum robot. In this chapter, the design, construction, and evaluation of a teleoperation input device designed for intuitive continuum manipulator teleoperation is presented.

4.1 Design and Construction

The MiniOct is a three-section continuum device that is capable of kinematically emulating a three-section, 9 DoF continuum slave device. The mechanical design of the device was inspired by the spring and cable system present in the Elephant Trunk manipulator [50]. The Elephant Trunk manipulator was an early continuum robot that utilized tendon actuation to bend. Springs allowed the manipulator to return to a straight, resting state. The MiniOct similarly uses tendons to hold curved shapes and springs to return to a resting state. The total system measures 71.59 cm in height and weighs approximately 1.57 kg. The device is comprised of two main hardware

components: the continuum input controller and the configuration measurement system. The two components can be seen in Figure 4.1, where section A is the continuum input controller and section B is the measurement system.

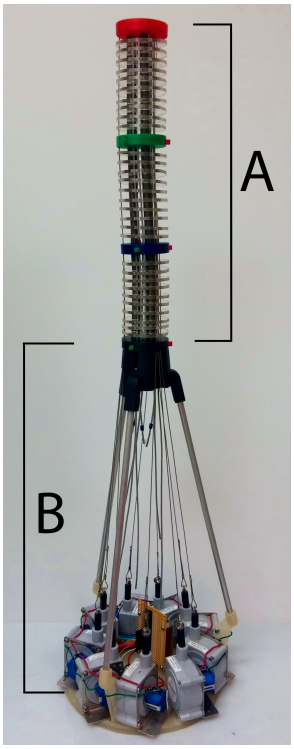

Figure 4.1: MiniOct Continuum Controller

4.1.1 Continuum Input Device

Similarly to [50], a parallel system of cables and springs allow the MiniOct to curve and extend with constant curvature for each of the 3 sections. Unlike the Elephant Trunk manipulator [50], which had 4 cables per section (2 opposing pairs at 90° radial spacing), the MiniOct only uses 3 springs and 3 cables per section arranged at 120° radial separation, similar to the actuation of the OctArm manipulator [42] it is designed to control. Additionally, the MiniOct is constructed with extension springs, whereas the Elephant Trunk used compression springs. This design difference means that the MiniOct's default configuration is compressed in its unactuated, straight, state as opposed to extended to the maximum device length of the Elephant Trunk manipulator. The length of the continuum controller section ranges from 31.75 cm to 57.16 cm.

A system of cables within each section use friction to maintain any configuration acheived from manipulation by a user. The friction imposed on each cable is created by placing spring loaded tabs at the base of each section. These tabs encircle the cables and press against them to prevent slipping in either direction. When pressed by a user, the springs release and the tabs allow the cable to glide freely, extending or compressing the side of the section immediately distal to the corresponding tab. A cross-section of a section divider with the tabs for each cable can be seen in Figure 4.2.

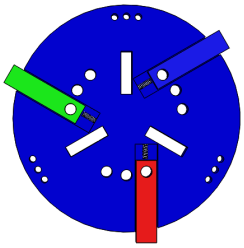

Figure 4.2: Cross Section of Push Tab System

The section dividers were printed on additive manufacturing devices (3D printers), and designed to be rotationally symmetric at intervals of 120 degrees with slots for the termination of section springs, holes for each cable, and internal tracks for the cable tabs. The section dividers are assigned different colors (red, green, and blue as seen in Figure 4.1) to help distinguish the sections for the operator. Also featured in each divider is a series of smaller holes that allow for the passage of thin cables attached to measurement devices that determine the configuration of the MiniOct. These devices are described in Section 4.1.2. In order to maintain constant curvature, each section is fitted with a series of acrylic spacers that keep the relative distance between the springs and cables constant. These spacers prevent buckling of the springs and force each section to curve in a smooth fashion, creating constant curvature for the cables. They are fixed at equal intervals along the extension springs using transparent cord. An example of a spacer for the base section can be seen in Figure 4.3.

4.1.2 Configuration Measurement

In order to use the MiniOct as a master device in the teleoperation of continuum manipulators, the device must be able to output information that can be used to determine the configuration

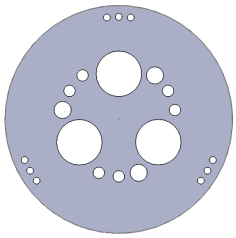

Figure 4.3: Acrylic Spacer for Base Section of MiniOct

of the device and thus the desired configuration of the slave robot. For the MiniOct, this information is provided in the form of 9 cable length measurements, 3 lengths for each section placed 120 degrees apart. These measurements are read as voltages, ranging from 0-5V, from a series of string potentiometers, which are placed symmetrically in a circle at the base of the device. The potentiometer configuration can be seen in Figure 4.4.

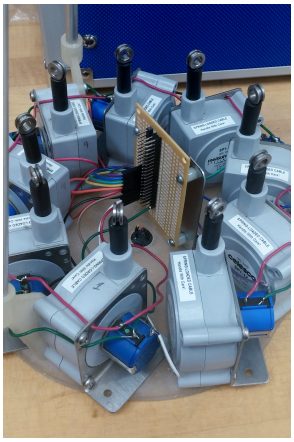

Figure 4.4: Ring of String Pots for Determining Configuration

The string potentiometers in use are voltage dividers that increase output signal in direct proportion to the length in which the string is extended. Each of the potentiometers is attached to a cable running along the length of the MiniOct and terminate at the end of the base, middle, or tip section. The output voltages are then converted to usable values using the following equations:

$$\ell_{bi} = (V_{bi})\frac{\Delta_{\ell b}}{V_{max}} + \ell_{bmin} \tag{4.1}$$

$$\ell_{mi} = (V_{mi} - V_{bi})\frac{\Delta_{\ell m}}{V_{max}} + \ell_{mmin} \tag{4.2}$$

$$\ell_{ti} = (V_{ti} - V_{mi} - V_{ti})\frac{\Delta_{\ell t}}{V_{max}} + \ell_{tmin} \tag{4.3}$$

where ℓ_{bi}, ℓ_{mi}, and ℓ_{ti} are the calculated output (desired for the slave device) lengths for the base, middle, and tip sections, respectively, of the slave device for the ith actuator in each section. V_{bi}, V_{mi}, and V_{ti} are the ouput voltages from the MiniOct string potentiometers, again corresponding to the base, middle, and tip sections for the ith string potentiometer for each section. $\Delta_{\ell b}$, $\Delta_{\ell m}$, and $\Delta_{\ell t}$ are the total change in length achievable by each section of the slave device and ℓ_{bmin}, ℓ_{mmin}, and ℓ_{tmin} are the minimum section lengths of the slave device. V_{max} is the maximum voltage that can be output from the MiniOct by fully extending a single section. The values of ℓ_{bi}, ℓ_{mi}, and ℓ_{ti} can be used to calculate desired values for the kinematics of a slave device and can be directly used to calculate slave device input such as pneumatic pressure or tendon length.

4.2 System Implementation

Following the development of the hardware and signal output, the device was tested by controlling the OctArm. The control values for the regulators are derived in a Simulink model [46]. In this procedure, the output from the MiniOct was obtained using the Quanser board and converted to OctArm section lengths within the same Simulink model used to control the OctArm. Once converted to lengths using Equations 4.1, 4.2, and 4.3, the values are used to calculate the necessary pressures to achieve the configuration designated by the MiniOct.

In order to increase the intuitiveness of the MiniOct's design, the device is color coded to allow a user to easily determine the relative orientation between the master and slave devices. In this experiment, the OctArm was similarly marked with blue, green, and red tape to indicate which of the base, middle, and tip sections, respectively, should be curving in response to the MiniOct configuration. Additional color labeling was used to determine orientation of the bending sections by corresponding to the colors of the push tabs on the master device. Figure 4.5 depicts the color coordination between the OctArm and MiniOct.

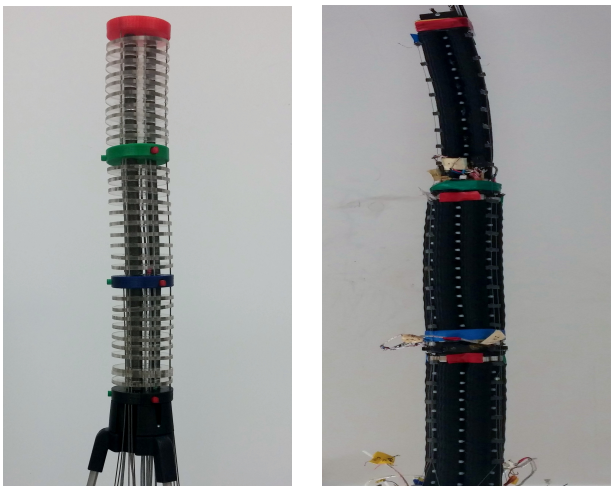

Figure 4.5: Color Coordination of Base, Middle, and Tip Sections

In order to demonstrate the functionality of the MiniOct, a series of configurations were reached that show the relationship between the MiniOct and the OctArm. Figure 4.6a and 4.6b demonstrate curving of a single section with two differing orientations. The first orientation is towards the view of the user while the second is perpendicular to the view. Figure 4.6c shows the actuation of the middle section while keeping the base and tip sections without curve or extension. Figure 4.6d is an example of curving two sections, each with a different orientation. The final configuration, seen in Figure 4.7, shows control of all 3 of the OctArm sections using the MiniOct.

As illustrated in Figure 4.6, the orientation of the slave device mirrors that of the MiniOct. In these experiments, this relationship between orientations was created for the clarity of the results. The motion of the slave device can be changed quickly to mirror or, alternatively, directly mimic the cofiguration of the MiniOct.

4.3 Discussion

The goal of this part of the work was to create a small, easy to use continuum device capable of acting as a master device for a 9 DoF continuum manipulator. The device needed to control extension and curving of three continuum sections in any direction. As seen in Section 4.2, the implementation of the MiniOct controller proved to be simple and very effective. Once constructed, the MiniOct operator was able to intuitively provide direct control a 9 DoF continuum manipulator with minimal calibration.

(a) Curving Tip Section (a)

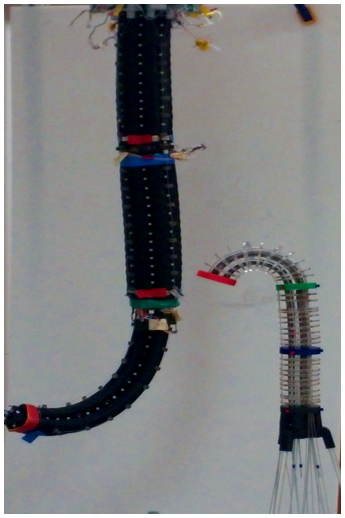

(b) Curving Tip Section (b)

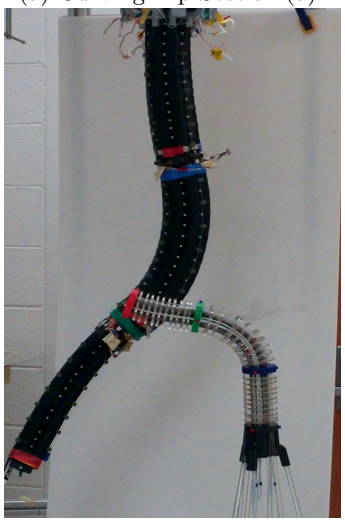

(c) Curving Middle Section

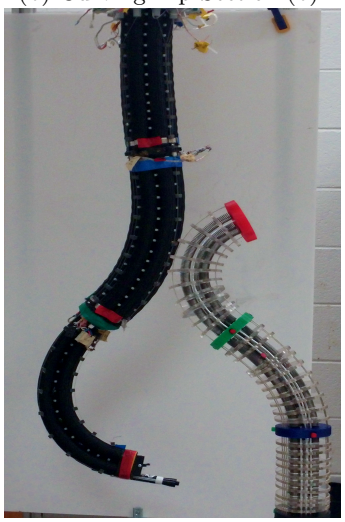

(d) Two Section Manipulation

Figure 4.6: Configurations between Master and Slave Device

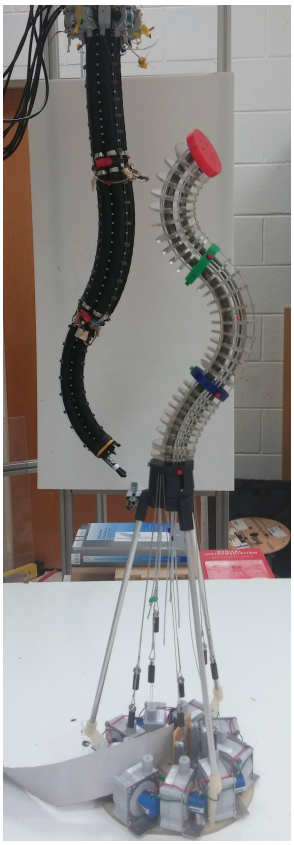

Figure 4.7: Three Section Control of Slave Device

While the final design provides ideal direct kinematic mapping, there are some limitations of the device to address. The cable system does well at maintaining the configuration set by the user but the friction imposed by the push tabs is not enough to overcome the spring loaded force of the string potentiometers for large extension of the base section. The base section is subject to the compression force of the three springs within its section and all 9 of the string potentiometers, producing more loading on the section. The middle and tip sections are able to hold their shape regardless of the extension length. In order to address this problem, the friction on the base cables needs to be increased. Two potential solutions are to increase the surface area of the contact with the push tabs or to use string potentiometers with reduced spring tension.

Additionally, the current design has all elements of the MiniOct exposed to the user. This creates a potential pinch hazard and increases the chance of damage to the device. While the open design makes repair simple, there is potential benefit to creating an extensible cover for sections. A cover could be developed using a thin rubber sheath, fabric, or other compliant material.

Another area of improvement is to develop a way to extend while maintaining curvature. The operation of the MiniOct allows for the extension and curving of a section, but once set to a curvature it is difficult to extend along that curve without first straightening out the MiniOct section. Design modifications to achieve this are currently being investigated.

While there are some hardware flaws to address, the potential for the MiniOct is significant. The versatility of the device allows for the control of any three section continuum device, regardless of length or actuation type. While the MiniOct was designed for the control of a pneumatic driven manipulator, the controller can also be built using compression springs in order to relate to tendon-driven devices that are fully extended at rest.

As noted earlier, no past teleoperation devices in the literature for continuum robots have been able to directly control all DoF of a slave device. The MiniOct is unique in having the ability the control the entire configuration of a continuum system and also intuitively provide control of the end-effector. The volume surrounding the MiniOct can be thought to represent a scaled model of the volume surrounding the slave device, including orientation if both devices are mounted in the same base orientation.

Further versatility of the MiniOct is present in the modularity of the sections. The current design has three distinct sections but additional sections could be added once the issue of friction is addressed in the base section. The MiniOct would then be able to control beyond the 9 DoF

currently present.

Chapter 5

Conclusion

This thesis presented a series of new results related to the teleoperation of continuum robots. Two major contributions were made, one in the development of teleoperation devices and techniques and the other main contribution was to the nonlinear control of planar continuum robots.

5.1 Summary of Contributions

Chapter 2 introduced a novel nonlinear control law for the teleoperation of extensible continuum robots. The control law is inspired by standard adaptive control techniques. However, the control law assumes no uncertainties in the model or the environment. Though the designed control law does not exactly cancel the slave dynamics, the results demonstrate that exponential tracking convergence is still achieved at a rate similar to exact cancellation. Results were demonstrated through both the simulation and physical implementation of a three section continuum manipulator.

Chapter 3 investigated a novel solution to the teleoperation of continuum robots through the use of a rigid-link robot as the control device. The study investigated the use of such a system in both planar and spatial motion. Fifteen volunteers tested the developed control mappings in order to gauge the intuitiveness of such a system. The teleoperation control scheme proved to be successful in allowing novice robotic users effective control of a continuum robot. There was no obvious relation between the robotic or video gaming experience of the participants and their success in manipulating the continuum robot. Though no mapping was universally perceived by the users to be intuitive, the results suggest that the use of rigid-link robots as teleoperative controllers is viable for continuum

systems.

The teleoperation of an extensible continuum robot through the use of a newly developed continuum input device was investigated in Chapter 4. A description of the design and construction of the input device is given. Device design allows for easy transportation and enables versatility of slave system. The device was used to control a nine degree-of-freedom continuum robot in spatial motion, demonstrating the capability of the system. The direct similarity in kinematics allowed for ease of use and intuitive control of the slave system. The user was able to relate orientation of master and slave device using visual cues from color of continuum sections.

5.2 Future Research

The results from the nonlinear controller experiments revealed desirable end-effector convergence of the slave continuum manipulator. However, each configuration required a varied set of tuned controller values in order to ensure stability and reduce system oscillations. Because of this, the system could not dynamically track the configuration set by the master device, instead reaching singular set points. The implementation of a Kalman filter or other gain tuning tool could allow for real time end-effector tracking between the master and slave devices.

The reported results only draw comparisons between the nonlinear controller and the open-loop control of the OctArm. A comparative study between other forms of system control such as proportional-derivative (PD) control or the sliding mode controller reported in [41] could reveal an optimal solution or point towards the need to further explore nonlinear control techniques in the teleoperation of planar continuum manipulators.

Oscillations seen in the experimental results of the nonlinear controller suggest uncertainties between the control model and the physical system. These uncertainties could be a difference of mass between the modeled and physical system. Additional simulations that investigate these potential model errors should be conducted, varying mass incrementally to discover the impact on modeled behavior.

The teleoperation trials involving the Kinova Mico and the OctArm in Chapter 3 revealed the need for a more intuitive input device for continuum robots. The MiniOct, introduced in Chapter 4, was designed to fulfill this need, but, at the time of writing, remains untested by novice users. Future efforts should attempt to evaluate the current solutions with a study similar to the study

reported in this thesis.

Additionally, solutions to incorporate additional system feedback, such as haptics, into the master device are being considered. This would enable the user to interact with more diverse environments and obtain more information about such environments than current teleoperation schemes allow. Inclusion of feedback to the operator would subsequently open a new area in continuum research concerned with the bilateral teleoperation of continuum systems.

Appendices

Appendix A

Teleoperation Trial Documents

Sample Demographic Data Survey

Q. Gender
What is your sex?
o Male
o Female

Q. Age
In what year were you born? ____

Q. Education
What is the highest degree or level of school ***you have completed***? If currently enrolled, mark the previous grade or highest degree received.
o High school graduate - high school diploma or the equivalent (for example: GED)
o Some college credit, but less than 1 year
o 1 or more years of college, no degree
o Associate degree (for example: AA, AS)
o Bachelor's degree (for example: BA, AB, BS)
o Master's degree (for example: MA, MS, MEng, MEd, MSW, MBA)
o Professional degree (for example: MD, DDS, DVM, LLB, JD)
o Doctorate degree (for example: PhD, EdD)

Q. Major
What major are you pursuing if currently enrolled, of if you have completed college-level education, what major(s) have you completed?_____

Q. Robotics Experience
How many years of experience operating robots do you have?
o None
o <1
o 1-3
o 4-6
o 7-10
o 11-15
o 16-20
o 20-30
o >30

Q. Video Games Experience
How many years of experience playing video games do you have?
o None
o<1
o 1-3
o 4-6
o 7-10
o 11-15
o 16-20
o 20-30
o >30

Evaluation Form:

Instructions: Please answer each question regarding the various teleoperation devices. You may rate each device on a scale from 0 to 100 (where 0 is impossible to use and 100 is intuitive to use). Feel free to write in your own number or choose from the labeled levels. **Please provide which control scheme is being graded in the blank space next to the question.**

Question 1: How accessible\learnable was the first teleoperation control scheme (_____)

Not at all Difficult but Useable Useable w/ Practice Useable Intuitive

0……25……50……75……100

Question 2: How accessible\learnable was the second teleoperation control scheme (_____)

Not at all Difficult but Useable Useable w/ Practice Useable Intuitive

0……25……50……75……100

Question 3: How accessible\learnable was the third teleoperation control scheme (_____)

Not at all Difficult but Useable Useable w/ Practice Useable Intuitive

0……25……50……75……100

Question 4: How accessible\learnable was the fourth teleoperation control scheme (_____)

Not at all Difficult but Useable Useable w/ Practice Useable Intuitive

0……25……50……75……100

Question 5: How accessible\learnable was the fifth teleoperation control scheme (_____)

Not at all Difficult but Useable Useable w/ Practice Useable Intuitive

0……25……50……75……100

Bibliography

[1] G. Niemeyer, C. Preusche, and G. Hirzinger, *Telerobotics*. Germany: Springer, 2008.

[2] G. Robinson and J. Davies, "Continuum robots - a state of the art," in *Proc. IEEE Int. Conf. Robot. Autom.*, Detroit, MI, 1999, pp. 2849–2854.

[3] D. Trivedi, C. Rahn, W. Kier, and I. Walker, "Soft robotics: Biological inspiration, state of the art, and future research," *Applied Bionics and Biomechanics*, vol. 5, no. 2, pp. 99–117, Jun. 2008.

[4] R. Webster III and B. A. Jones, "Design and modeling of constant curvature continuum robots," *Int. Jour. Robots. Res.*, vol. 29, no. 13, pp. 1661–1683, Jul. 2010.

[5] I. Walker, "Continuous backbone "continuum" robot manipulators: A review," *ISRN Robotics*, vol. 2013, no. 1, pp. 1–19, Jul. 2013.

[6] E. Butler, R. Hammond-Oakley, S. Chawarski, A. Gosline, P. Codd, T. Anor, J. Madsen, P. Dupont, and J. Lock, "Robotic neuro-endoscope with concentric tube augmentation," in *Proc. IEEE/RSJ Int. Conf. Intel. Robot. Syst.*, Vilamoura, Portugal, 2012, pp. 2941–2946.

[7] Y. Chen, J. Liang, and I. Hunter, "Modular continuum robotic endoscope design and path planning," in *Proc. IEEE Int. Conf. Robot. Autom.*, Hong Kong, China, 2014, pp. 5393–5398.

[8] N. Simaan, R. Taylor, and P. Flint, "A dextrous system for laryngeal surgery," in *Proc. IEEE Int. Conf. Robot. Autom.*, New Orleans, LA, 2004, pp. 351–357.

[9] R. Buckingham, "Snake arm robots," *Ind. Robot: An Int. Jour.*, vol. 29, no. 3, pp. 242–245, Mar. 2002.

[10] J. Mehling, M. Diftler, M. Chu, and M. Valvo, "A minimally invasive tendril robot for in-space inspection," in *Proc Biorobotics Conference*, Pisa, Italy, 2006, pp. 690–695.

[11] M. Tonapi, I. Godage, A. Vijaykumar, and I. Walker, "Spatial kinematic modeling of a long and thin continuum robotic cable," in *Proc. IEEE Int. Conf. Robot. Autom.*, Seattle, WA, 2015, pp. 3755–3761.

[12] C. Laschi, B. Mazzolai, V. Mattoli, M. Cianchetti, and P. Dario, "Design of a biomimetic robotic octopus arm," *Bioinsp. and Biomim.*, vol. 4, no. 1, pp. 1–8, Jan. 2009.

[13] D. Lane, B. Davies, G. Robinson, D. O'Brien, J. Sneddon, E. Seaton, and A. Elfstrom, "Aspects of the design and development of a subsea dextrous grasping system," *IEEE Jour. Ocean. Eng.*, vol. 24, no. 1, pp. 96–111, Jan. 1999.

[14] B. Jones and I. Walker, "Kinematics of multisection continuum robots," *IEEE Trans. Robot.*, vol. 22, no. 1, pp. 43–57, Feb. 2006.

[15] T. Mahl, A. Hildebrandt, and O. Sawodny, "A variable curvature continuum kinematics for kinematic control of the bionic handling assistant," *IEEE Transactions on Robotics*, vol. 30, no. 4, pp. 935–949, 2014.

[16] G. Chirikjian, "Hyper-redundant manipulator dynamics: A continuum approximation," *Adv. Robot.*, vol. 9, no. 3, pp. 217–243, Jun. 1995.

[17] R. Kang, A. Kazakidi, E. Guglielmino, D. Branson, D. Tsakiris, J. Ekaterinaris, and D. Caldwell, "Dynamic modeling of a hyper-redundant octopus-like manipulator for underwater applications," in *Proc. IEEE/RSJ Int. Conf. Intel. Robot. Syst.*, San Francisco, CA, 2011, pp. 4054–4059.

[18] G. Gallot, O. Ibrahimand, and W. Khalil, "Dynamic modeling and simulation of a 3-d eel-like robot," in *Proc. IEEE Int. Conf. Robot. Autom.*, Rome, Italy, 2007, pp. 1486–1491.

[19] A. Marchese, R. Tedrake, and D. Rus, "Dynamics and trajectory optimization for a soft spatial fluidic elastomer manipulator," in *Proc. IEEE Int. Conf. Robot. Autom.*, Seattle, WA, 2015, pp. 2528–2535.

[20] H. Mochiyama and T. Suzuki, "Kinematics and dynamics of a cable-like hyper-flexible manipulator," in *Proc. IEEE Int. Conf. Robot. Autom.*, Taipei, Taiwan, 2003, pp. 3672–3677.

[21] E. Tatlicioglu, I. Walker, and D. Dawson, "Dynamic modeling for planar extensible continuum robot manipulators," *Int. Jour. Robot. Autom.*, vol. 24, no. 4, pp. 1087–1099, Apr. 2009.

[22] M. Mahvash and P. Dupont, "Stiffness control of a continuum manipulator in contact with a soft environment," in *Proc. IEEE/RSJ Int. Conf. Intel. Robot. Syst.*, Taipei, Taiwan, 2010, pp. 863–870.

[23] D. Rucker, B. Jones, and R. Webster III, "A model for concentric tubes continuum robots under applied wrenches," in *Proc. IEEE Int. Conf. Robot. Autom.*, Anchorage, AK, 2010, pp. 1047–1052.

[24] J. Li and J. Xiao, "Task-constrained continuum manipulation in cluttered space," in *Proc. IEEE Int. Conf. Robot. Autom.*, Hong Kong, China, 2014, pp. 2183–2188.

[25] L. Lyons, R. Webster III, and R. Alterovitz, "Planning active cannula configurations through tubular anatomy," in *Proc. IEEE Int. Conf. Robot. Autom.*, Anchorage, AK, 2010, pp. 2082–2087.

[26] D. Palmer and S. C.-G. D. Axinte, "Real-time method for tip following navigation of continuum snake arm robots," *Robotics and Autonomous Systems*, vol. 62, no. 10, pp. 1478–1485, 2014.

[27] L. Torres, C. Baykal, and R. Alterovitz, "Interactive-rate motion planning for concentric tube robots," in *Proc. IEEE Int. Conf. Robot. Autom.*, Hong Kong, China, 2014, pp. 1914–1919.

[28] B. Conrad and M. Zinn, "Closed loop task space control of an interleaved continuum rigid manipulator," in *Proc. IEEE Int. Conf. Robot. Autom.*, Seattle, WA, 2015, pp. 1743–1750.

[29] V. Falkenhahn, A. Hildebrandt, R. Neumann, and O. Sawodny, "Model-based feedforward position control of constant curvature continuum robots using feedback linearization," in *Proc. IEEE Int. Conf. Robot. Autom.*, Seattle, WA, 2015, pp. 762–767.

[30] R. Goldman, A. Bajo, and N. Simaan, "Compliant motion control for multisegment continuum robots with actuation force sensing," *IEEE Trans. Rob.*, vol. 30, no. 4, pp. 890–902, Apr. 2014.

[31] A. Kapadia, K. Fry, and I. Walker, "Empirical investigation of closed-loop control of extensible continuum manipulators," in *Proc. IEEE Int. Conf. Intell. Robot. Sys.*, Chicago, IL, 2014, pp. 329–335.

[32] S. Sadati, Y. Noh, S. Naghibi, and A. Althoefer, "Stiffness control of soft robotic manipulators for minimally invasive surgery (mis) using scale jamming," in *Int. Conf. Rob. and Autom.*, Amsterdam, The Netherlands, 2015, pp. 141–151.

[33] M. Yip and D. Camarillo, "Model-less feedback control of continuum manipulators in constrained environments," *IEEE Trans. Rob.*, vol. 30, no. 4, pp. 880–888, Apr. 2014.

[34] M. Csencsits, B. Jones, and W. McMahan, "User interfaces for continuum robot arms," in *Proc. IEEE Int. Conf. Intell. Robot. Sys*, Edmonton, Canada, 2005, pp. 3011–3018.

[35] A. Kapadia, I. Walker, and E. Tatlicioglu, "Teleoperation control of a redundant continuum manipulator using a non-redundant rigid-link master," in *Proc. IEEE Int. Conf. Intell. Robot. Sys.*, Algarve, Portugal, 2012, pp. 3105–3110.

[36] I. Gravagne and I. D. Walker, "Manipulability, force, and compliance analysis for planar continuum manipulators," *IEEE Trans. Robots. Autom.*, vol. 18, no. 3, pp. 263–273, Jun. 2002.

[37] R. Scott, "Continuum surrogate software interface for teleoperation of continuum robots," Master's thesis, Clemson University, 2016.

[38] J. Hartranft, "Nonlinear model based control of robotic systems," Master's thesis, Clemson University, 2000.

[39] Y. Huang and T. Kuo, "Robust control for nonlinear time-varying systems with application to a robotic manipulator," *Int. J. of Sys. Sci.*, vol. 33, no. 10, pp. 831–837, 2002.

[40] A. Behal, W. Dixon, D. Dawson, and B. Xian, *Lyapunov-Based Control of Robotic Systems.* Boca Raton, FL, USA: CRC Press, 2009.

[41] A. Kapadia, I. Walker, D. Dawson, and E. Tatlicioglu, "A new approach to extensible continuum robot control using the sliding-mode," *Intl. J. Comp. Tech. and App.*, vol. 2, no. 4, pp. 293–300, 2011.

[42] M. Grissom, V. Chitrakaran, D. Dienno, M. Csencsits, M. Pritts, B. Jones, W. McMahan, D. Dawson, C. Rahn, and I. Walker, "Design and experimental testing of the octarm soft robot manipulator," in *Proc. SPIE Conf. Unmanned Sys. Tech.*, Kissimee, FL, 2006, pp. 109–114.

[43] F. L. Lewis, D. M. Dawson, and C. T. Abdallah, *Robot Manipulator Control: Theory and Practice.* New York, NY: Marcel Dekker, 2004.

[44] B. Jones and I. Walker, "A new approach to jacobian formulation for a class of multi-section continuum robots," in *Proc. IEEE Int. Conf. Robot. Autom.*, Barcelona, Spain, 2004, pp. 3279–3284.

[45] B. A. Jones, W. McMahan, and I. D. Walker, "Design and analysis of a novel pneumatic manipulator," in *Proc. IFAC Symposium on Mechatronic Systems*, Sydney, Australia, 2004, pp. 745–750.

[46] MathWorks. (2016, April) Simulation and model based design. [Online]. Available: http://www.mathworks.com/products/simulink

[47] Quanser. (2015, September) Q8-usb data acquisition board. [Online]. Available: http://www.quanser.com/products/q8-usb

[48] Kinova. (2015, September) Kinova mico research arm. [Online]. Available: www.kinovarobotics.com/service-robotics/products/robot-arms/

[49] C. Frazelle, A. Kapadia, K. Fry, and I. Walker, "Teleoperation mappings from rigid link robots to their extensible continuum counterparts," in *Proc. IEEE Int. Conf. Robot. Autom.*, Stockholm, Sweden, 2016.

[50] I. Walker and M. Hannan, "A novel 'elephant's trunk' robot," in *Proc. IEEE/ASME Int. Conf. Adv. Intel. Mechatronics*, Atlanta, GA, 1999, pp. 410–415.